AIAA JOURNAL
Vol. 39, No. 5, May 2001

Dereverberation and Its Application to Damage Detection in One-Dimensional Structures

Jun Ma* and Darryll J. Pines†
University of Maryland, College Park, Maryland 20742

The vibratory response of a structure can be represented by the superposition of traveling waves propagating along a complex structural network. Wave dynamics generated at natural boundary conditions and subsequently reflected at geometric boundary conditions can lead to pole-zero characteristics of conventional reverberated transfer functions. However, by implementing model-based wave virtual controllers at each structural element, a dereverberated transfer function can be obtained from the measured reverberated transfer function response. Because the dereverberated transfer function represents the direct path of energy transmission across a structure, it can be used to infer damage in a structure by tracking how variations in local element properties affect the propagation of incident energy through the structure. A methodology is presented for obtaining the dereverberated transfer function response for four types of structural elements, including symmetric and asymmetric discrete spring mass elements and spectral rod and beam finite elements for continuous structures. The dereverberated transfer function response is obtained by attaching virtual controllers at the terminals of each structural element. A phase damage index method is proposed based on the relative phase propagation error from element to element to quantify the type and amount of damage. Analytical results on several simulated examples confirm that the dereverberated response can be used as a method for locating and quantifying damage in structures.

Nomenclature

EA	=	axial stiffness
EI	=	bending stiffness
F	=	external point force
G_{bl}	=	wave controller attached to the left end of a beam
G_{br}	=	wave controller attached to the right end of a beam
G_d	=	wave controller for discrete spring mass system
G_r	=	wave controller for rod
i	=	imaginary unit $\sqrt{-1}$
k	=	spring stiffness
m	=	lumped mass
n	=	number of degree of freedom
t	=	time instant
u	=	axial displacement
v	=	vertical displacement
W_{le}	=	leftward evanescent wave component
W_{lp}	=	leftward propagating wave component
W_{re}	=	rightward evanescent wave component
W_{rp}	=	rightward propagating wave component
θ	=	angular displacement
ρA	=	mass per unit length
μ	=	wave number
ω	=	angular frequency

I. Introduction

THE extraction of the modal parameters of a structure for model-based damage detection methods has received a considerable amount of attention in the literature.[1] Many of these modal-based methods have found wide application to problems associated with structural health monitoring of aerospace, civil, and mechanical systems. However, studies have shown that these methods have many limitations, including sensitivity to model uncertainty, changes in boundary conditions, insensitivity to incipient structural defects, and sensor and actuator placement.[2,3] To counter these inherent problems, attention has focused on the development of alternative modeling approaches that can describe the vibratory motion of structures under external excitation. One such approach is to represent the response of a structure in terms of the superposition of traveling waves that can traverse individual elements of a structure, reflecting off boundaries to establish standing waves from constructive interference. These standing waves constitute the resonance or reverberant response of the structure and lead to reverberated transfer functions (RTF) from force excitation to sensor outputs. Common attributes of such frequency-domain responses are characteristic pole-zero patterns for collocated and noncollocated transfer functions. When these frequency-response functions are used, many methods[4] have been developed to obtain modal properties of a variety of structures. However, often neglected in the process is that these RTF responses comprise the steady-state superposition of incident and reflected traveling waves propagating along the structure. These traveling wave components can be used to identify local damage in structural systems.

The idea of identifying damage using the scattering of transient structural waves[5,6] is directly related to the dereverberated response of a structure. Whereas the RTF of a structure measures the response when traveling waves interfere constructively and destructively with each other, the dereverberated transfer function (DTF) is a measure of the steady-state response of a structure when incident waves do not reflect off internal or external boundaries. Thus, the characteristic pole-zero behavior commonly found in RTF responses is suppressed in favor of the mean or backbone response of the RTF transfer function. The DTF response essentially represents the steady-state incident power flowing through the structure from each actuator to each sensor.

Initial attempts to suppress broadband vibration of structural waves involved ad hoc feedforward and local feedback control laws.[7–12] MacMartin and Hall[9] found that the optimal collocated feedback controller had noncausal properties that were not physically realizable with conventional analog electronic components. However, many researchers[11,12] have developed a series of approximate collocated controllers that were physically realizable but not optimal in terms of dissipation of energy. Such collocated controllers were demonstrated experimentally to reduce the resonant response of uniform structures over a fairly broad frequency range involving several modes of a structure. These approximate controllers were later used in an initial study[13] to infer qualitatively the presence of delamination damage in several tapered composite rotorcraft

Received 30 June 2000, revision received 1 December 2000; accepted for publication 4 December 2000.

*Graduate Research Assistant, Smart Structures Laboratory, Alfred Gessow Rotorcraft Center, Department of Aerospace Engineering; junma@eng.umd.edu.

†Associate Professor, Smart Structures Laboratory, Alfred Gessow Rotorcraft Center, Department of Aerospace Engineering; djpterp@eng.umd.edu. Associate Fellow AIAA.

flexbeam specimens using the DTF response. This paper develops the precise mathematical formalism for determining the matched terminating controllers required between successive nonuniform structural elements to obtain the DTF from the RTF response at every degree of freedom. The DTF is used to infer the presence and location of damage by examining the relative phase lag error between successive degrees of freedom. A damage index method is introduced to quantify the amount and type of damage (mass or stiffness) occurring in a particular structural element. One-dimensional examples illustrate that the presence, location, and amount of local damage can be determined in discrete and continuous structures.

In the next section of this paper the concept of dereverberation is introduced, followed by a discussion on how to obtain the DTF response of discrete and continuous structural elements. In Sec. III, the DTF response is obtained on simulated nonuniform discrete and continuous structures. Finally, in Sec. IV, a damage detection method using the DTF response and a phase damage index method illustrate the effectiveness of the approach.

II. DTFs of Structural Elements

A. Discrete Spring–Mass Elements

Discrete spring–mass structures can be constructed from two types of elements: symmetric and asymmetric.[14] A symmetric element is shown in Fig. 1a. It has identical masses m at both ends of the element connected by a spring with stiffness k in the middle. An asymmetric element is shown in Fig. 1b and has only one mass attached to either end of the spring. A generic spring–mass element is shown in Fig. 1c. Notice that when $m_1 = m_2$, the generic elements are symmetric elements. When $m_1 = 0$, they are asymmetric elements. This section introduces an approach to obtain DTFs for asymmetric spring–mass elements and for generic spring–mass elements.

1. *Asymmetric Spring–Mass Element*

The equations of motion of the asymmetric spring–mass element shown in Fig. 1b are

$$k(x_1 - x_2) = F_1, \qquad m\ddot{x}_2 + k(x_2 - x_1) = F_2 \tag{1}$$

Assuming a solution of the form

$$x_n(t) = Ae^{i\omega t - n\mu} \qquad n = 1, 2 \tag{2}$$

where n is the degree of freedom (DOF) of interest, leads to the following expressions for the wave numbers μ_L and μ_R:

$$\mu_L = \mu = \cosh^{-1}[(2k - m\omega^2)/2k]$$
$$\mu_R = -\mu = -\cosh^{-1}[(2k - m\omega^2)/2k] \tag{3}$$

where subscripts L and R refer to the leftward and rightward propagation coefficients. Therefore, the spectral representation for the longitudinal displacements of each DOF are

$$\hat{x}_1(\omega) = W_{\mathrm{rp}}(\omega)e^{-\mu} + W_{\mathrm{lp}}(\omega)e^{\mu}$$
$$\hat{x}_2(\omega) = W_{\mathrm{rp}}(\omega)e^{-2\mu} + W_{\mathrm{lp}}(\omega)e^{2\mu} \tag{4}$$

Assume that energy is input from the left with $F_1 \neq 0$. A controller can be added at the right to extract energy out. The control force is designed to have the form $F_{2c} = G_d x_2$ and must satisfy two objectives: 1) ensure equilibrium of forces at DOF x_2 and 2) prevent energy reflection between the elements. Therefore, the control force F_{2c} must satisfy the following equations:

$$F_{2m} + F_{2c} = 0, \qquad W_{\mathrm{lp}}(\omega) = 0 \tag{5}$$

where F_{2m} is the motion-dependent force. From the first part of Eq. (5), we have

$$m\ddot{x}_2 + k(x_2 - x_1) + G_d x_2 = 0 \tag{6}$$

Transformed into the frequency domain, Eq. (6) becomes

$$-m\omega^2\hat{x}_2 + k(\hat{x}_2 - \hat{x}_1) + \hat{G}_d\hat{x}_2 = 0 \tag{7}$$

Now substitute Eq. (4) into Eq. (7) and set $W_{\mathrm{lp}} = 0$. After some algebra the control gain is determined to be

$$\hat{G}_d = m\omega^2 - k + ke^{\mu} \tag{8}$$

If the RTF matrix of an asymmetric element is available, transfer functions $\hat{x}_1/\hat{F}_1$ and $\hat{x}_2/\hat{F}_1$ can be dereverberated by using the following expression:

$$\begin{bmatrix} \hat{x}_1/\hat{F}_1 \\ \hat{x}_2/\hat{F}_1 \end{bmatrix}_{\mathrm{DTF}} = \left(\mathrm{RTF}^{-1} + \begin{bmatrix} 0 & 0 \\ 0 & \hat{G}_d \end{bmatrix}\right)^{-1} \begin{bmatrix} 1 \\ 0 \end{bmatrix} \tag{9}$$

The RTF and DTF responses of $\hat{x}_1/\hat{F}_1$ and $\hat{x}_2/\hat{F}_1$ are shown in Figs. 2a and 2b, respectively. As expected, the effect of the control force F_{2c} is to remove the resonance and antiresonance from the response. The control gain for the asymmetric structural elements are plotted vs ω in Fig. 2c. Notice that this compensator has an unusual magnitude and phase behavior that is not consistent with conventional linear pole-zero representations. The magnitude behavior for the compensator has a derivative-type characteristic up until the cutoff frequency. However, the phase is not necessarily equal to 90 deg. Thus, such a compensator would be difficult to implement with conventional electric components.

2. *Generic Structural Elements*

When the generic element shown in Fig. 1c is considered, energy is input from the left in terms of $F_1 \neq 0$. A control force F_{2c} is applied at the right end to prevent energy reflection. This generic element can be seperated into two parts, shown in Fig. 1d.

Figure 1d shows the force boundary condition. The equation of motion at DOF x_1 is given by

$$F_1 = m_1\ddot{x}_1 + F_w \tag{10}$$

where F_w, is the force that generates a wave propagating through k and m_2. The control force $F_{2c} = G_d x_2$ prevents energy that arrives at m_2 from being reflected. From the discussion in the preceding section, the controller gain G_d is determined only by parameters m_2 and k. The control gain is independent of F_w, which means it is independent of m_1. Mass m_1, joined by F_1, determines the speed and amplitude of energy passing through the element, but has nothing to do with the controller applied at the right end to obtain the nonresonant transfer functions. If the conventional RTF matrix of the generic element is known, transfer functions $\hat{x}_1/\hat{F}_1$ and $\hat{x}_2/\hat{F}_1$ can be dereverberated using the following expression:

$$\begin{bmatrix} \hat{x}_1/\hat{F}_1 \\ \hat{x}_2/\hat{F}_1 \end{bmatrix}_{\mathrm{DTF}} = \left(\mathrm{RTF}^{-1} + \begin{bmatrix} 0 & 0 \\ 0 & \hat{G}_d \end{bmatrix}\right)^{-1} \begin{bmatrix} 1 \\ 0 \end{bmatrix} \tag{11}$$

The DTF responses $\hat{x}_1/\hat{F}_1$ and $\hat{x}_2/\hat{F}_1$ corresponding to different m_1 and m_2 values are shown in Fig. 3.

B. Continuous Structural Elements

Whereas discrete spring–mass structural elements can be used to model a variety of complex structures, continuous structural elements are also being used to model structures such as space trusses, rotor blades, and buildings. In this section, models of rod and beam elements are developed. When the concept of a virtual controller

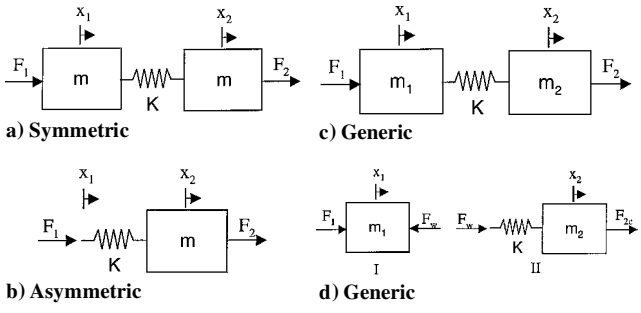

Fig. 1 Discrete spring–mass elements.

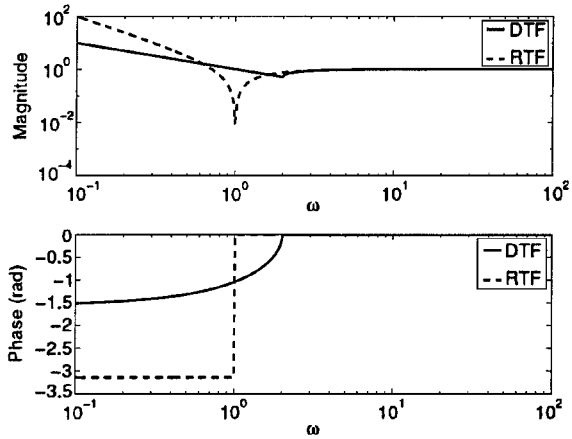

a) RTF and DTF responses of $\hat{x}_1/\hat{F}_1$

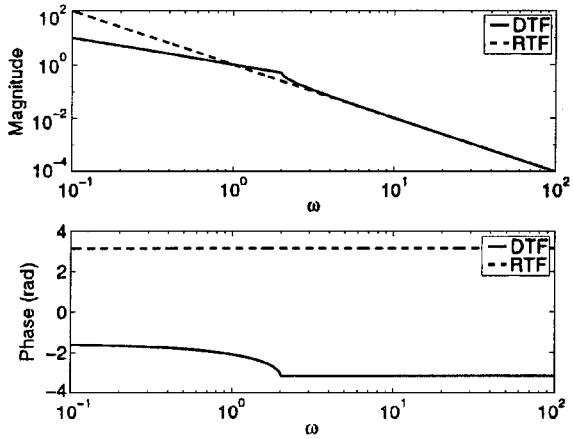

b) RTF and DTF responses of $\hat{x}_2/\hat{F}_1$

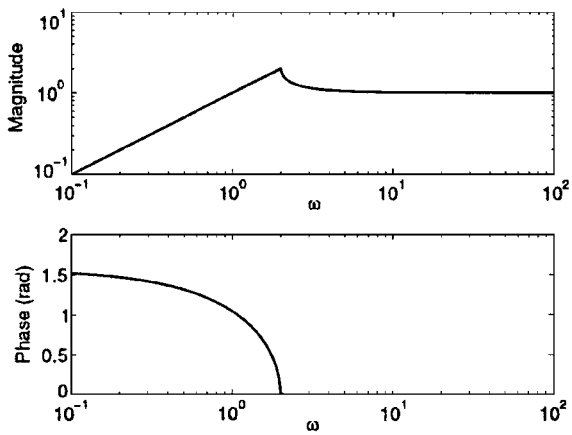

c) Control gain $\hat{G}_d$

Fig. 2 Asymmetric element: 0.01% damping assumed, $k_2 = 1$ N/m, and $m_2 = 1$ kg.

is used, the dereverberated response is obtained for continuous rod and beam spectral elements.

1. Uniform Rod Element

A uniform rod element is shown in Fig. 4a. The equation of motion for a rod is given by

$$EA\frac{\partial^2 u(x,t)}{\partial x^2} - \rho A\frac{\partial^2 u(x,t)}{\partial t^2} = f(x,t) \tag{12}$$

Transformed into the frequency domain, Eq. (12) becomes

$$EA\frac{\partial^2 \hat{u}(x,\omega)}{\partial x^2} + \rho A\omega^2 \hat{u}(x,\omega) = \hat{f}(x,\omega) \tag{13}$$

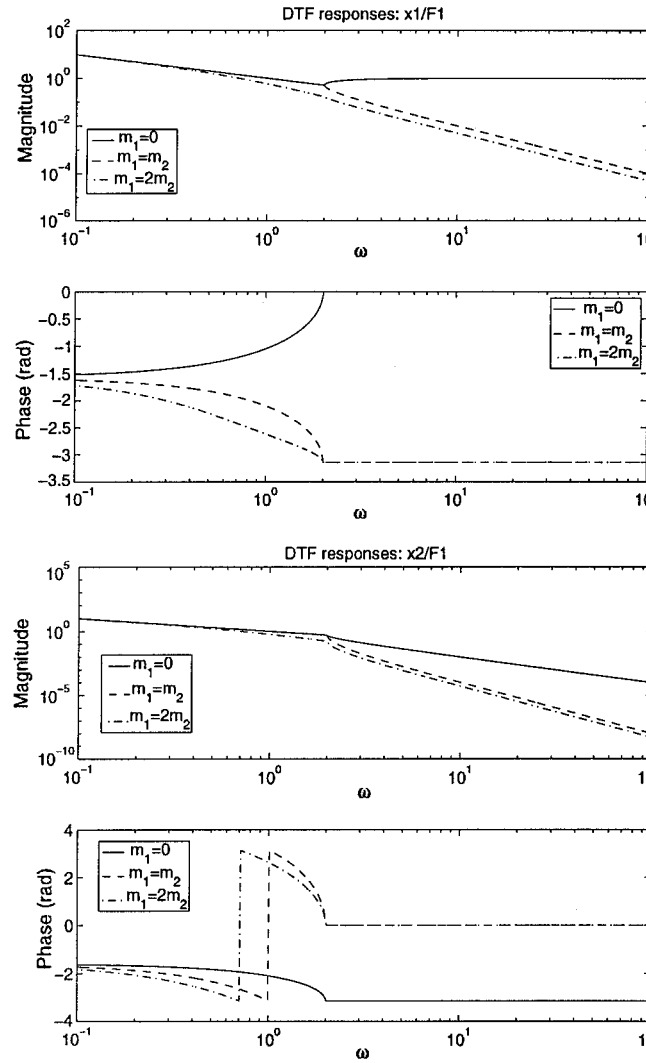

Fig. 3 DTF responses of generic elements.

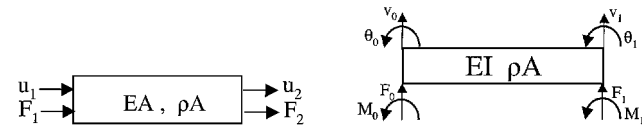

a) Uniform rod **b) Uniform beam**

Fig. 4 Element.

The spectral representation[15] for the longitudinal deflection of the rod is given by

$$\hat{u}(x,\omega) = W_{\mathrm{rp}}(\omega)e^{-i\mu x} + W_{\mathrm{lp}}(\omega)e^{-i\mu(L-x)} \tag{14}$$

where $\mu = \omega\sqrt{(\rho A/EA)}$ is the longitudinal wave number. Assume that energy is input from the left end with $F_1 \neq 0$. As the incident energy arrives at the right end, a control force $F_{2c} = G_r u_2$ is designed to satisfy two objectives: 1) ensure equilibrium of the forces at the right end and 2) prevent energy reflection at the right end. Therefore, the control force must satisfy

$$F_{2m} + F_{2c} = 0, \qquad W_{\mathrm{lp}}(\omega) = 0 \tag{15}$$

where

$$F_{2m} = EA\frac{\partial \hat{u}}{\partial \hat{x}}\bigg|_{x=L}$$

is the motion-dependent force. After some algebra, the control gain is determined to be

$$\hat{G}_r = i\mu EA \tag{16}$$

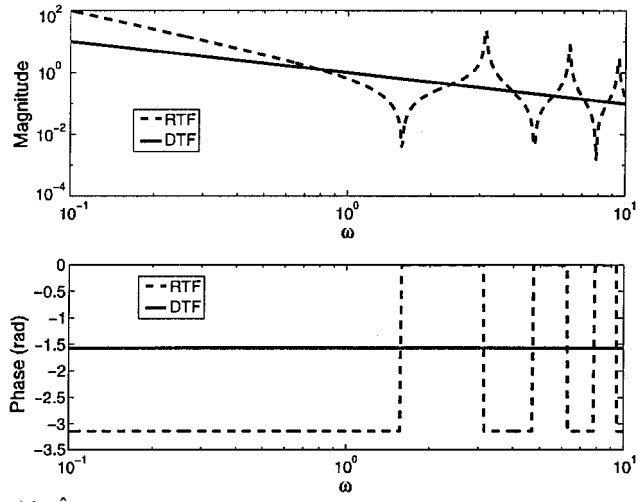

a) $\hat{u}_1/\hat{F}_1$

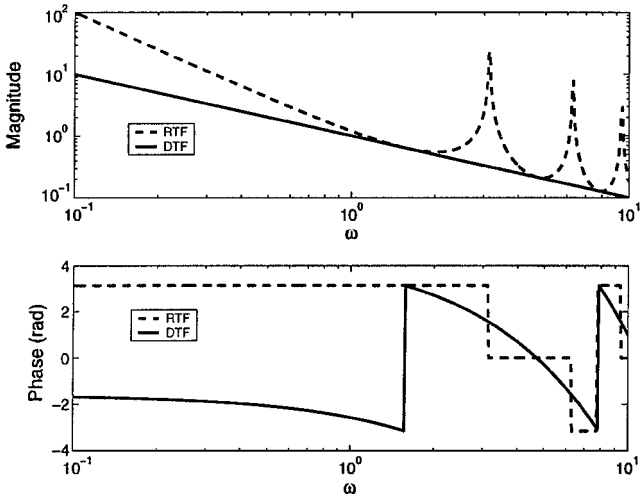

b) $\hat{u}_2/\hat{F}_1$

Fig. 5 RTF and DTF responses of uniform rod element with 0.01% damping assumed and $EA = 1$ N, $\rho A = 1$ kg/m, and $L = 1$ m.

If the RTF matrix of a uniform rod element is available, the DTFs $\hat{u}_1/\hat{F}_1$ and $\hat{u}_2/\hat{F}_1$ can be obtained using the following expression:

$$\begin{bmatrix} \hat{u}_1/\hat{F}_1 \\ \hat{u}_2/\hat{F}_1 \end{bmatrix}_{\text{DTF}} = \left(\text{RTF}^{-1} + \begin{bmatrix} 0 & 0 \\ 0 & \hat{G}_r \end{bmatrix} \right)^{-1} \begin{bmatrix} 1 \\ 0 \end{bmatrix} \tag{17}$$

The DTF and RTF responses of $\hat{u}_1/\hat{F}_1$ and $\hat{u}_2/\hat{F}_1$ are shown in Fig. 5.

Note that transfer functions $\hat{u}_1/\hat{F}_2$ and $\hat{u}_2/\hat{F}_2$ are not dereverberated by Eq. (17). These transfer functions can be dereverberated by

$$\begin{bmatrix} \hat{u}_1/\hat{F}_2 \\ \hat{u}_2/\hat{F}_2 \end{bmatrix}_{\text{DTF}} = \left(\text{RTF}^{-1} + \begin{bmatrix} \hat{G}_r & 0 \\ 0 & 0 \end{bmatrix} \right)^{-1} \begin{bmatrix} 0 \\ 1 \end{bmatrix} \tag{18}$$

2. Uniform Beam Element

A uniform beam element is shown in Fig. 4b. The equation of motion for a Bernouli–Euler beam is given by

$$EI \frac{\partial^4 v(x,t)}{\partial x^4} + \rho A \frac{\partial^2 v(x,t)}{\partial t^2} = f(x,t) \tag{19}$$

Transformed into frequency domain, Eq. (19) becomes

$$EI \frac{\partial^4 \hat{v}(x,\omega)}{\partial x^4} - \rho A \omega^2 \hat{v}(x,\omega) = \hat{f}(x,\omega) \tag{20}$$

The spectral representation for the beam's flexural vibration are

$$\begin{aligned} \hat{v} &= W_{\text{rp}} e^{-i\mu x} + W_{\text{re}} e^{-\mu x} + W_{\text{lp}} e^{-i\mu(L-x)} + W_{\text{le}} e^{-\mu(L-x)} \\ \hat{\theta} &= W_{\text{rp}}(-i\mu) e^{-i\mu x} + W_{\text{re}}(-\mu) e^{-\mu x} + W_{\text{lp}}(i\mu) e^{-i\mu(L-x)} \\ &\quad + W_{\text{le}}(\mu) e^{-\mu(L-x)} \end{aligned} \tag{21}$$

where $\mu = [(\rho A/EI)\omega^2]^{1/4}$ is the bending wave number. Different sign conventions lead to different expressions of nodal displacements and nodal forces. The sign convention applied here is shown in Fig. 4b. Nodal displacements are given by

$$\begin{bmatrix} v_0 \\ \theta_0 \\ v_1 \\ \theta_1 \end{bmatrix} = \begin{bmatrix} 1 & 1 & e^{-i\mu L} & e^{-\mu L} \\ -i\mu & -\mu & i\mu e^{-i\mu L} & \mu e^{-\mu L} \\ e^{-i\mu L} & e^{-\mu L} & 1 & 1 \\ -i\mu e^{-i\mu L} & -\mu e^{-\mu L} & i\mu & \mu \end{bmatrix} \begin{bmatrix} W_{\text{rp}} \\ W_{\text{re}} \\ W_{\text{lp}} \\ W_{\text{le}} \end{bmatrix} \tag{22}$$

Nodal forces

$$F_{0m} = EI \frac{\partial^3 v}{\partial x^3}\bigg|_{x=0}, \qquad M_{0m} = -EI \frac{\partial^2 v}{\partial x^2}\bigg|_{x=0}$$

$$F_{1m} = -EI \frac{\partial^3 v}{\partial x^3}\bigg|_{x=L}, \qquad M_{1m} = EI \frac{\partial^2 v}{\partial x^2}\bigg|_{x=L}$$

are motion dependent and are given by

$$\begin{bmatrix} F_{0m} \\ M_{0m} \\ F_{1m} \\ M_{1m} \end{bmatrix} = EI\mu^2 \begin{bmatrix} i\mu & -\mu & -i\mu e^{-i\mu L} & \mu e^{-\mu L} \\ 1 & -1 & e^{-i\mu L} & -e^{-\mu L} \\ -i\mu e^{-i\mu L} & \mu e^{-\mu L} & i\mu & -\mu \\ -e^{-i\mu L} & e^{-\mu L} & -1 & 1 \end{bmatrix} \begin{bmatrix} W_{\text{rp}} \\ W_{\text{re}} \\ W_{\text{lp}} \\ W_{\text{le}} \end{bmatrix} \tag{23}$$

When it is assumed that energy is input from the left, control forces

$$\begin{bmatrix} F_{1c} \\ M_{1c} \end{bmatrix} = G_{\text{br}} \begin{bmatrix} v_1 \\ \theta_1 \end{bmatrix} \tag{24}$$

are applied at the right end to satisfy the following equations:

$$\begin{bmatrix} F_{1c} \\ M_{1c} \end{bmatrix} + \begin{bmatrix} F_{1m} \\ M_{1m} \end{bmatrix} = \begin{bmatrix} 0 \\ 0 \end{bmatrix}, \qquad \begin{bmatrix} W_{\text{lp}}(\omega) \\ W_{\text{le}}(\omega) \end{bmatrix} = \begin{bmatrix} 0 \\ 0 \end{bmatrix} \tag{25}$$

Solving for the control gain leads to

$$\hat{G}_{\text{br}} = \begin{bmatrix} (i-1)EI\mu^3 & iEI\mu^2 \\ iEI\mu^2 & (1+i)EI\mu \end{bmatrix} \tag{26}$$

When this matrix control law is used, the DTFs can be obtained from

$$\begin{bmatrix} \hat{v}_0/\hat{F}_0 & \hat{v}_0/\hat{M}_0 \\ \hat{\theta}_0/\hat{F}_0 & \hat{\theta}_0/\hat{M}_0 \\ \hat{v}_1/\hat{F}_0 & \hat{v}_1/\hat{M}_0 \\ \hat{\theta}_1/\hat{F}_0 & \hat{\theta}_1/\hat{M}_0 \end{bmatrix}_{\text{DTF}} = \left(\text{RTF}^{-1} + \begin{bmatrix} 0_{2\times 2} & 0_{2\times 2} \\ 0_{2\times 2} & \hat{G}_{\text{br}} \end{bmatrix} \right)^{-1} \begin{bmatrix} 1 & 0 \\ 0 & 1 \\ 0 & 0 \\ 0 & 0 \end{bmatrix} \tag{27}$$

The DTF and RTF response for $\hat{v}_0/\hat{F}_0$, $\hat{v}_0/\hat{M}_0, \ldots, \hat{\theta}_1/\hat{F}_0$, $\hat{\theta}_1/\hat{M}_0$ are shown in Fig. 6.

If the energy is from the right, different control forces

$$\begin{bmatrix} F_{0c} \\ M_{0c} \end{bmatrix} = \hat{G}_{\mathrm{bl}} \begin{bmatrix} v_0 \\ \theta_0 \end{bmatrix} \tag{28}$$

are applied at the left end to satisfy the following equations:

$$\begin{bmatrix} F_{0c} \\ M_{0c} \end{bmatrix} + \begin{bmatrix} F_{0m} \\ M_{0m} \end{bmatrix} = \begin{bmatrix} 0 \\ 0 \end{bmatrix}, \qquad \begin{bmatrix} W_{\mathrm{rp}}(\omega) \\ W_{\mathrm{re}}(\omega) \end{bmatrix} = \begin{bmatrix} 0 \\ 0 \end{bmatrix} \tag{29}$$

The control gains are given by

$$\hat{G}_{\mathrm{bl}} = \begin{bmatrix} (i-1)EI\mu^3 & -iEI\mu^2 \\ -iEI\mu^2 & (1+i)EI\mu \end{bmatrix} \tag{30}$$

The DTFs are obtained from

$$\begin{bmatrix} \hat{v}_0/\hat{F}_1 & \hat{v}_0/\hat{M}_1 \\ \hat{\theta}_0/\hat{F}_1 & \hat{\theta}_0/\hat{M}_1 \\ \hat{v}_1/\hat{F}_1 & \hat{v}_1/\hat{M}_1 \\ \hat{\theta}_1/\hat{F}_1 & \hat{\theta}_1/\hat{M}_1 \end{bmatrix}_{\mathrm{DTF}} = \left(\mathrm{RTF}^{-1} + \begin{bmatrix} \hat{G}_{\mathrm{bl}} & 0_{2\times 2} \\ 0_{2\times 2} & 0_{2\times 2} \end{bmatrix} \right)^{-1} \begin{bmatrix} 0 & 0 \\ 0 & 0 \\ 1 & 0 \\ 0 & 1 \end{bmatrix} \tag{31}$$

Remember that the controllers attached at both ends of rod elements are the same. However, in the case of a beam, the controller gain matrices $\hat{G}_{\mathrm{br}}$ and $\hat{G}_{\mathrm{bl}}$ have a sign difference in the off-diagonal terms. This is because the sign convention that was used for the beam did not create a symmetric element stiffness matrix.

III. DTF Responses of Nonuniform Structures

A. Discrete Spring–Mass Structures

1. Energy Input from End

A five-DOF spring–mass structure is shown in Fig. 7a. The properties of this structure are listed in Table. 1. Complex stiffness is used to add a small amount of damping to the structure and to overcome potential numerical problems. The right end of this structure is fixed and the left end is free. Energy is input from the left in terms of $F_1 \neq 0$. The reverberated transfer function matrix RTF of this structure is given by

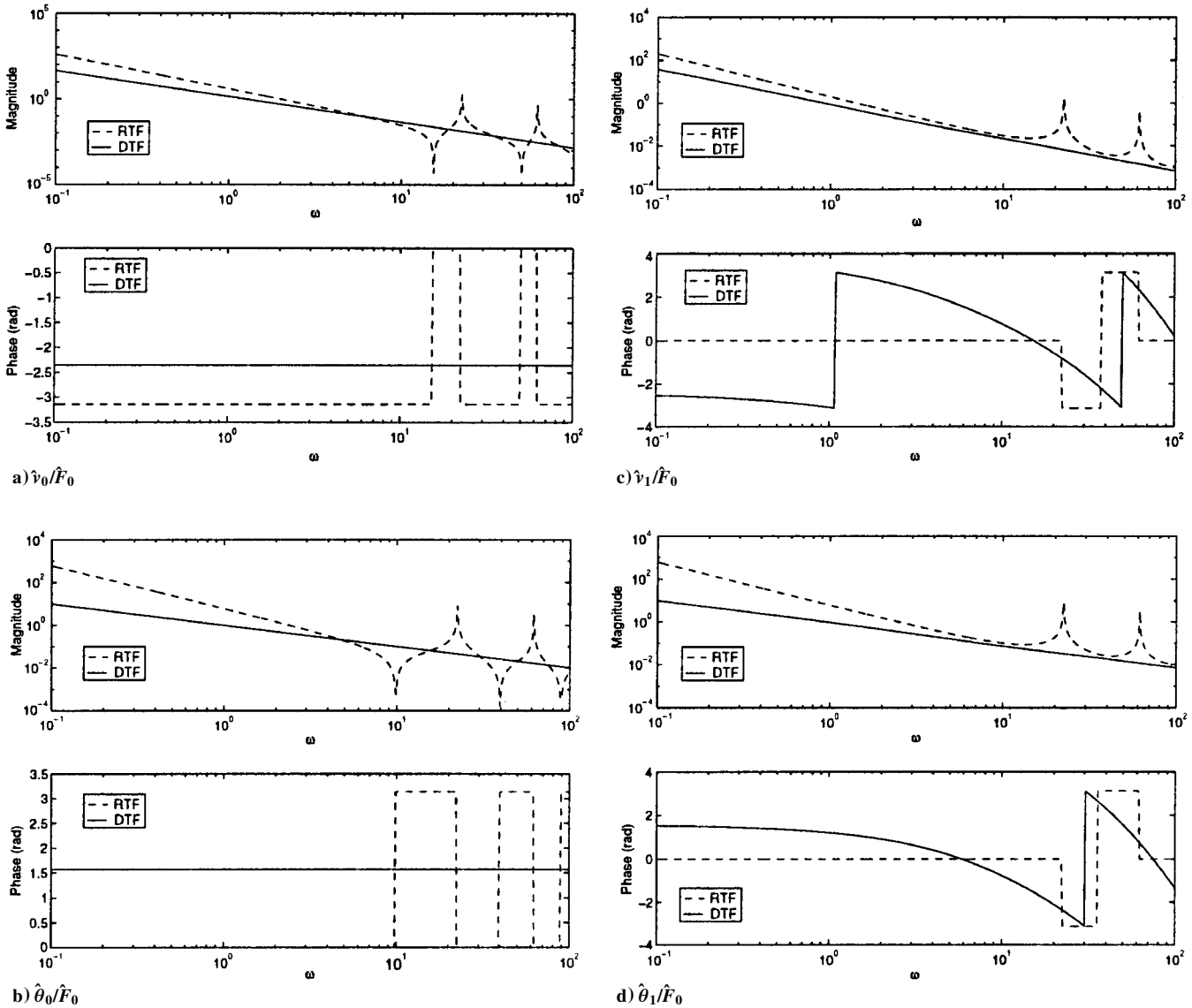

Fig. 6 RTF and DTF responses.

$$\begin{bmatrix}\hat{x}_1\\ \hat{x}_2\\ \hat{x}_3\\ \hat{x}_4\\ \hat{x}_5\end{bmatrix} = \mathrm{RTF}\begin{bmatrix}\hat{F}_1\\ \hat{F}_2\\ \hat{F}_3\\ \hat{F}_4\\ \hat{F}_5\end{bmatrix} = \begin{bmatrix}k_1 - m_1\omega^2 & -k_1 & 0 & 0 & 0\\ -k_1 & k_1 + k_2 - m_2\omega^2 & -k_2 & 0 & 0\\ 0 & -k_2 & k_2 + k_3 - m_3\omega^2 & -k_3 & 0\\ 0 & 0 & -k_3 & k3 + k_4 - m_4\omega^2 & -k_4\\ 0 & 0 & 0 & -k_4 & k_4 + k_5 - m_5\omega^2\end{bmatrix}^{-1}\begin{bmatrix}\hat{F}_1\\ \hat{F}_2\\ \hat{F}_3\\ \hat{F}_4\\ \hat{F}_5\end{bmatrix} \tag{32}$$

To obtain the DTFs with respect to external force F_1, the structural part to the right of mass m_5 will be ignored. This has been done for two reasons: First, the original wave has already passed all DOF after it arrives at m_5. Structural components behind m_5 along the wavelength will be ignored because DTF deals with the incident wave. Second, the fixed boundary condition should be ignored, otherwise it will generate a reflective wave. The control scheme to obtain DTF responses is shown in Fig. 7b. F_w is derived from the force boundary condition at the left. Local controllers are used to match the impedance of adjacent elements. Thus, there is no energy reflection at the interface of different elements. Mathematically, the DTFs for $\hat{x}_1/\hat{F}_1, \hat{x}_2/\hat{F}_1, \ldots, \hat{x}_5/\hat{F}_1$ can be found using the following expression:

$$\begin{bmatrix}\hat{x}_1/\hat{F}_1\\ \hat{x}_2/\hat{F}_1\\ \hat{x}_3/\hat{F}_1\\ \hat{x}_4/\hat{F}_1\\ \hat{x}_5/\hat{F}_1\end{bmatrix}_{\mathrm{DTF}} = \left(\mathrm{RTF}^{-1} + \begin{bmatrix}0 & 0 & 0 & 0 & 0\\ 0 & G_{2d} - G_{3d} & 0 & 0 & 0\\ 0 & 0 & G_{3d} - G_{4d} & 0 & 0\\ 0 & 0 & 0 & G_{4d} - G_{5d} & 0\\ 0 & 0 & 0 & 0 & G_{5d} - k_5\end{bmatrix}\right)^{-1}\begin{bmatrix}1\\ 0\\ 0\\ 0\\ 0\end{bmatrix} \tag{33}$$

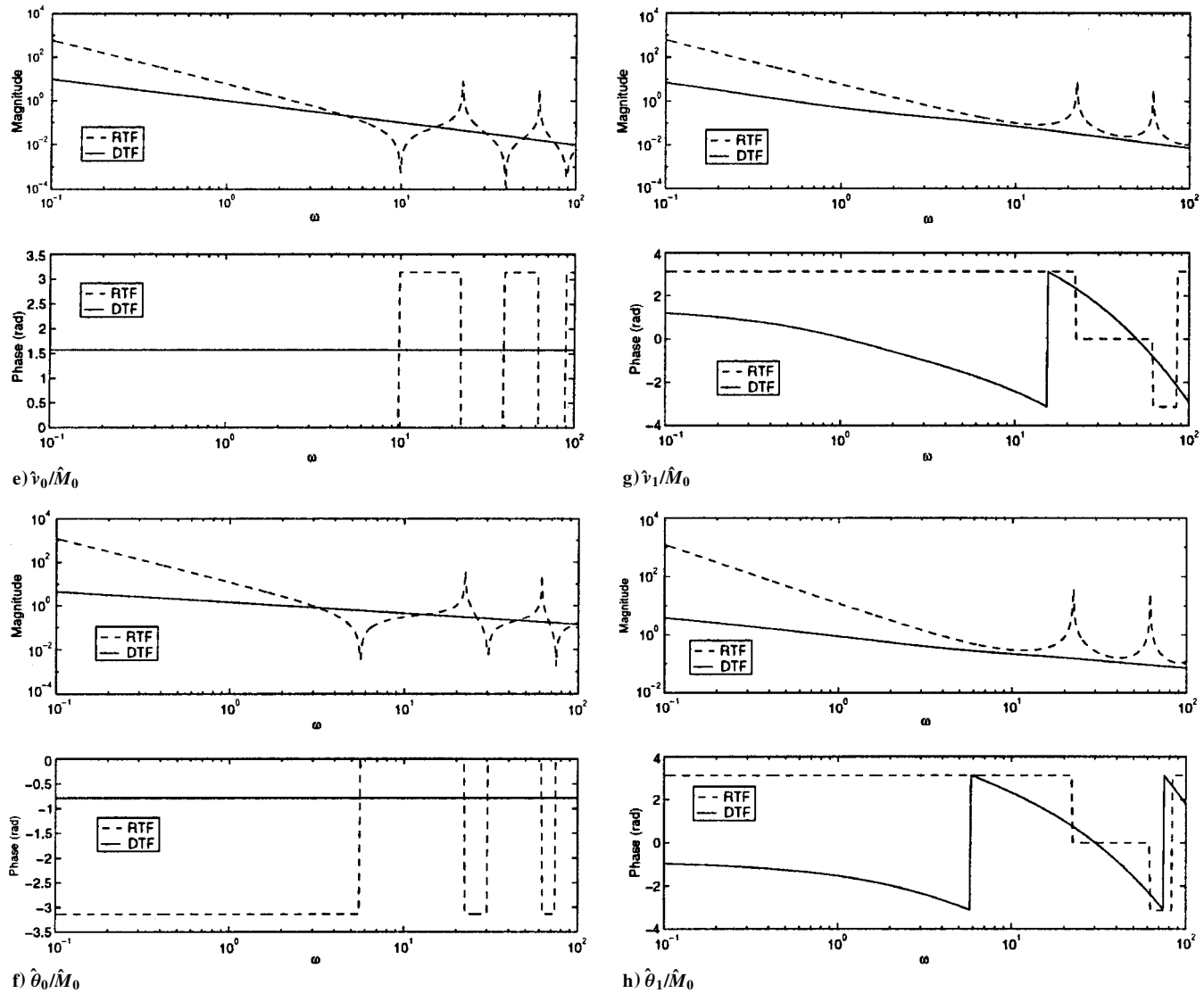

Fig. 6 RTF and DTF responses (continued).

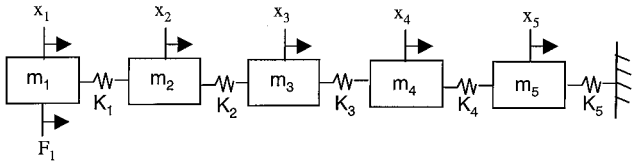

Fig. 7a Spring–mass structure with five DOF.

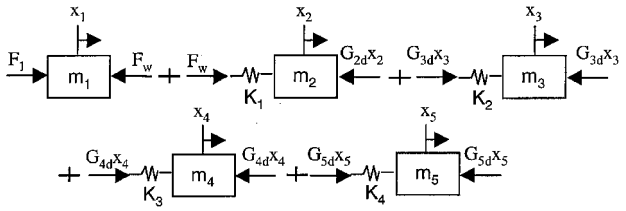

Fig. 7b Control scheme to obtain DTF responses.

where $G_{nd} = m_n\omega^2 - k_{n-1} + k_{n-1}e^{\mu_n}$ and $\mu_n = \cosh^{-1}[(2k_{n-1} - m_n\omega^2)/2k_{n-1}]$. Now we know the DTF responses of $\hat{x}_1/\hat{F}_1$, $\hat{x}_2/\hat{F}_1, \ldots, \hat{x}_5/\hat{F}_1$. For damage detection purpose, we are more interested in how an individual element affects a wave passing through it. This is demonstrated by DTF responses $(\hat{x}_{n+1})/\hat{x}_n$, $n = 1, 2, \ldots, 4$ of successive DOF. These transfer function responses are shown in Fig. 8.

2. Energy Input from Middle

A five-DOF spring–mass structure with energy input at the middle ($F_3 \neq 0$) is shown in Fig. 9a. Spring stiffness k_5 and the fixed end will be ignored to obtain the DTF responses. Hence, this structure can be thought to be constructed from two parts, shown in Fig. 9b. Each part reveals the path of incident wave propagating along both directions, respectively. Adding these two parts together, an alternate structure is used to obtain the DTF of original structure with respect to input F_3 (see Fig. 9c).

The RTF response of the original structure shown in Fig. 9a is given by

Table 1 Properties of the five-DOF spring–mass structure[a]

	i				
Property	1	2	3	4	5
k_i, N/m	20	10	10	20	30
m_i, kg	2	2	1	3	1

[a] Assuming 0.01% damping.

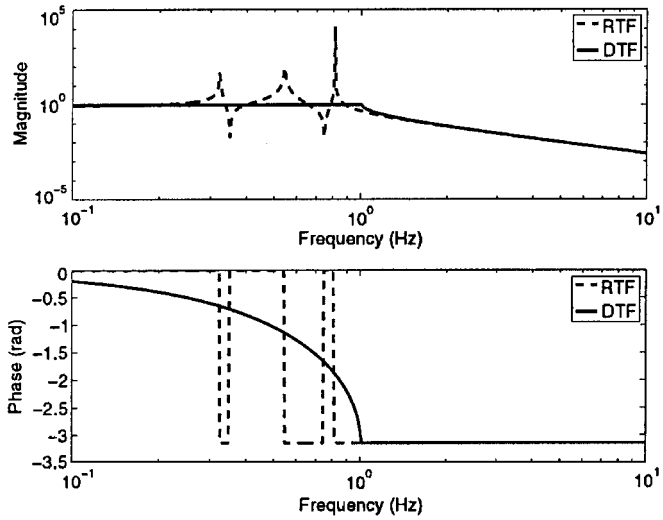

a) $\hat{x}_2/\hat{x}_1$

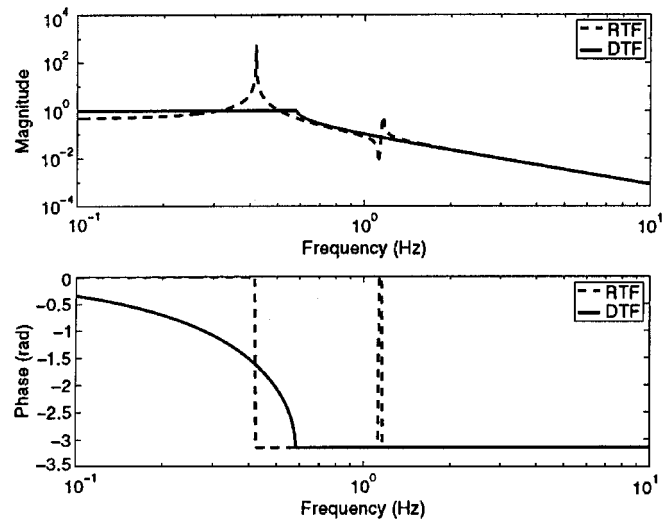

c) $\hat{x}_4/\hat{x}_3$

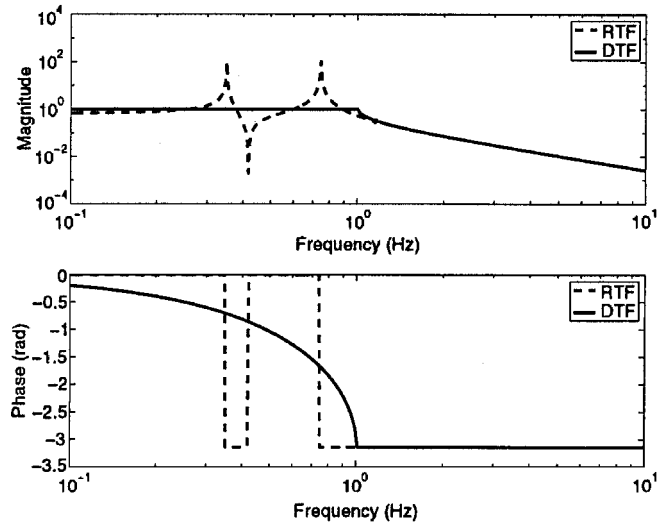

b) $\hat{x}_3/\hat{x}_2$

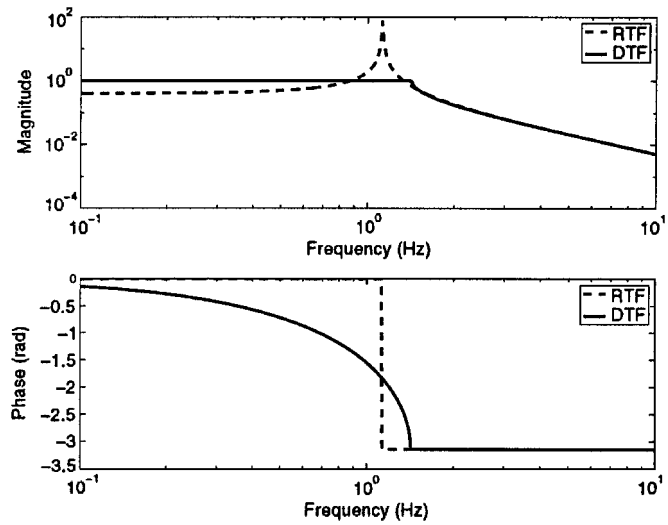

d) $\hat{x}_5/\hat{x}_4$

Fig. 8 DTF and RTF responses.

$$\mathrm{RTF} = \begin{bmatrix} k_1 - m_1\omega^2 & -k_1 & 0 & 0 & 0 \\ -k_1 & k_1 + k_2 - m_2\omega^2 & -k_2 & 0 & 0 \\ 0 & -k_2 & k_2 + k_3 - m_3\omega^2 & -k_3 & 0 \\ 0 & 0 & -k_3 & k3 + k_4 - m_4\omega^2 & -k_4 \\ 0 & 0 & 0 & -k_4 & k_4 + k_5 - m_5\omega^2 \end{bmatrix}^{-1} \tag{34}$$

Notice that the alternate structure is different from the original structure in two ways: 1) The spring attached to fixed end k_5 is ignored. 2) The mass at the external force acting point is twice m_3. Thus, transfer functions $\hat{x}_1/F_3$, $\hat{x}_2/F_3$, ..., $\hat{x}_5/F_3$ can be dereverberated using the following expression:

$$\begin{bmatrix} \hat{x}_1/\hat{F}_3 \\ \hat{x}_2/\hat{F}_3 \\ \hat{x}_3/\hat{F}_3 \\ \hat{x}_4/\hat{F}_3 \\ \hat{x}_5/\hat{F}_3 \end{bmatrix}_{\mathrm{DTF}} = \left(\mathrm{RTF}^{-1} + \begin{bmatrix} G_{1d} & 0 & 0 & 0 & 0 \\ 0 & G_{2d} - G_{1d} & 0 & 0 & 0 \\ 0 & 0 & -m_3\omega^2 & 0 & 0 \\ 0 & 0 & 0 & G_{4d} - G_{5d} & 0 \\ 0 & 0 & 0 & 0 & G_{5d} - k_5 \end{bmatrix} \right)^{-1} \times \begin{bmatrix} 0 \\ 0 \\ 1 \\ 0 \\ 0 \end{bmatrix} \tag{35}$$

Similarly, the DTF transfer functions $\hat{x}_1/\hat{x}_2$, $\hat{x}_2/\hat{x}_3$, $\hat{x}_4/\hat{x}_3$, and $\hat{x}_5/\hat{x}_4$ can be obtained and are shown in Fig. 10.

B. Nonuniform Continuous Structures

The mechanism used to obtain DTF responses for rodlike structures is similar to the one applied to spring–mass structures developed in preceding sections. In this section, beam structures developed from spectral elements are discussed, and methods for obtaining the DTF response from the RTF response are illustrated for nonuniform continuous structural models.

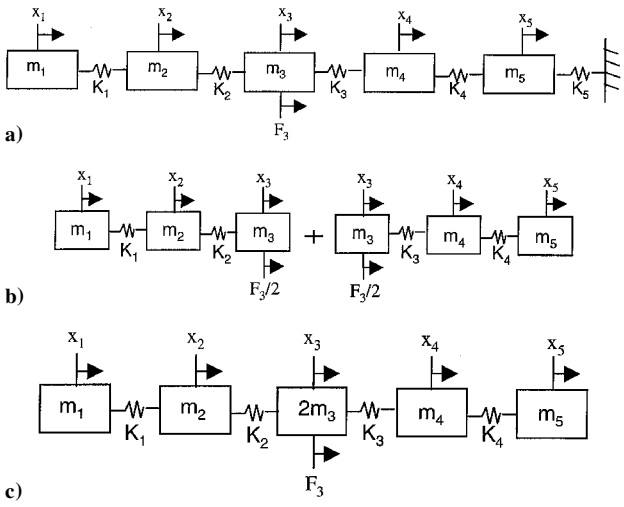

Fig. 9 Spring–mass structure with five DOF.

1. *Free–Free Beam*

A free–free beam composed of five spectral elements is shown in Fig. 11a. When spectral finite element analysis[15] is used, the element stiffness matrix of each element is given by

$$\begin{bmatrix} F_{n-1} \\ M_{n-1} \\ F_n \\ M_n \end{bmatrix} = \begin{bmatrix} k^n_{11}(\omega) & k^n_{12}(\omega) & k^n_{13}(\omega) & k^n_{14}(\omega) \\ k^n_{21}(\omega) & k^n_{22}(\omega) & k^n_{23}(\omega) & k^n_{24}(\omega) \\ k^n_{31}(\omega) & k^n_{32}(\omega) & k^n_{33}(\omega) & k^n_{34}(\omega) \\ k^n_{41}(\omega) & k^n_{42}(\omega) & k^n_{43}(\omega) & k^n_{44}(\omega) \end{bmatrix} \begin{bmatrix} v_{n-1} \\ \theta_{n-1} \\ v_n \\ \theta_n \end{bmatrix} = \begin{bmatrix} K^n_1 & K^n_2 \\ K^n_3 & K^n_4 \end{bmatrix} \begin{bmatrix} v_{n-1} \\ \theta_{n-1} \\ v_n \\ \theta_n \end{bmatrix} \tag{36}$$

where $n = 1, \ldots, 5$ and K^n_1, K^n_2, K^n_3, and K^n_4 are 2×2 matrices.

The spectral finite element model of the entire beam can be constructed to obtain

$$\begin{bmatrix} F_0 \\ M_0 \\ F_1 \\ M_1 \\ F_2 \\ M_2 \\ F_3 \\ M_3 \\ F_4 \\ M_4 \\ F_5 \\ M_5 \end{bmatrix} = \begin{bmatrix} K^1_1 & K^1_2 & & & & \\ K^1_3 & K^1_4 + K^2_1 & K^2_2 & & 0 & \\ & K^2_3 & K^2_4 + K^3_1 & K^3_2 & & \\ & & K^3_3 & K^3_4 + K^4_1 & K^4_2 & \\ & 0 & & K^4_3 & K^4_4 + K^5_1 & K^5_2 \\ & & & & K^5_3 & K^5_4 \end{bmatrix} \times \begin{bmatrix} v_0 \\ \theta_0 \\ v_1 \\ \theta_1 \\ v_2 \\ \theta_2 \\ v_3 \\ \theta_3 \\ v_4 \\ \theta_4 \\ v_5 \\ \theta_5 \end{bmatrix} \tag{37}$$

where off-diagonal elements of this banded matrix are zero.

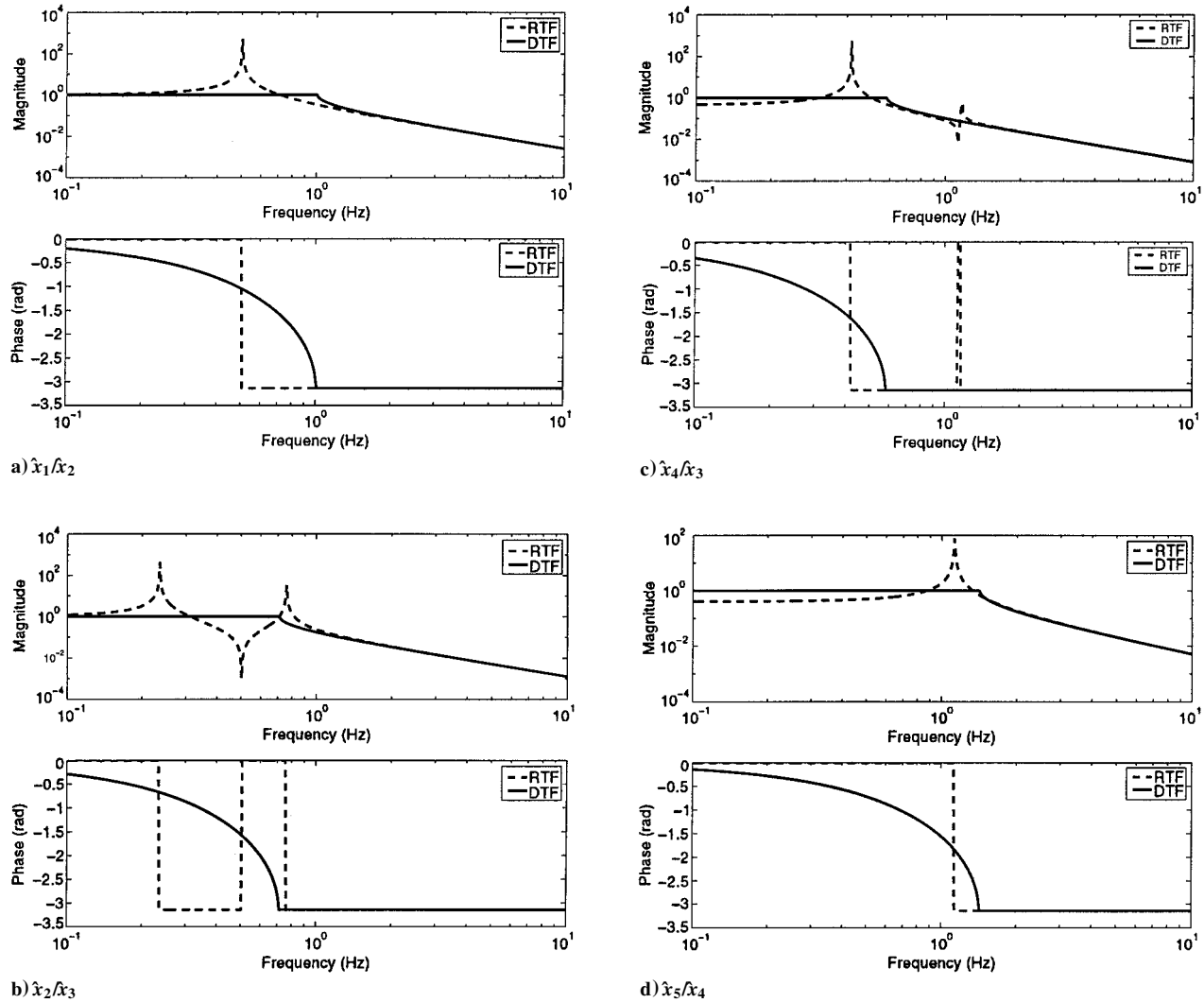

a) $\hat{x}_1/\hat{x}_2$ c) $\hat{x}_4/\hat{x}_3$

b) $\hat{x}_2/\hat{x}_3$ d) $\hat{x}_5/\hat{x}_4$

Fig. 10 DTF and RTF responses.

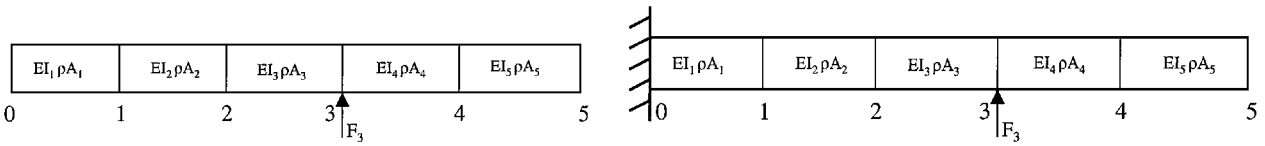

a) Free-free b) Fixed-free

Fig. 11 Five element beam.

The conventional reverberated transfer function matrix RTF can be obtained experimentally and satisfies

$$\mathrm{RTF} = \begin{bmatrix} K_1^1 & K_2^1 & & & & \\ K_3^1 & K_4^1 + K_1^2 & K_2^2 & & 0 & \\ & K_3^2 & K_4^2 + K_1^3 & K_2^3 & & \\ & & K_3^3 & K_4^3 + K_1^4 & K_2^4 & \\ & 0 & & K_3^4 & K_4^4 + K_1^5 & K_2^5 \\ & & & & K_3^5 & K_4^5 \end{bmatrix}^{-1} \tag{38}$$

Assume the energy is input from the middle of the beam where the vertical force $F_3 \neq 0$. DTFs $v_0/F_3, \theta_0/F_3, v_1/F_3, \theta_1/F_3, \ldots, v_5/F_3$, and θ_5/F_3 can be obtained by attaching noncausal controllers to all nodes except the actuation point. This process is shown in Fig. 12. Mathematically, it can be expressed as

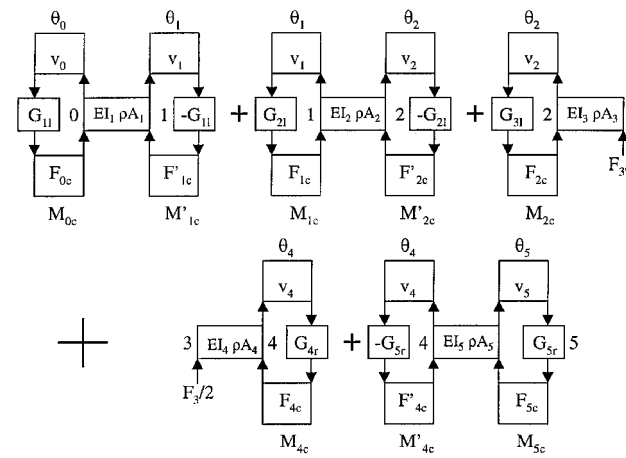

Fig. 12 Applying local feedback controllers to obtain DTF of a nonuniform beam structure.

$$\begin{bmatrix} v_0/F_3 \\ \theta_0/F_3 \\ v_1/F_3 \\ \theta_1/F_3 \\ v_2/F_3 \\ \theta_2/F_3 \\ v_3/F_3 \\ \theta_3/F_3 \\ v_4/F_3 \\ \theta_4/F_3 \\ v_5/F_3 \\ \theta_5/F_3 \end{bmatrix}_{\text{DTF}} = \left(\text{RTF}^{-1} + \begin{bmatrix} G_{1l} & & & & & \\ & G_{2l} - G_{1l} & & & 0 & \\ & & G_{3l} - G_{2l} & & & \\ & & & 0_{2\times 2} & & \\ & 0 & & & G_{4r} - G_{5r} & \\ & & & & & G_{5r} \end{bmatrix} \right)^{-1} \begin{bmatrix} 0 \\ 0 \\ 0 \\ 0 \\ 0 \\ 0 \\ 1 \\ 0 \\ 0 \\ 0 \\ 0 \\ 0 \end{bmatrix} \tag{39}$$

The process shown in Fig. 12 is actually a terminal matching process. Energy is input at node 3 in terms of $F_3 \neq 0$. The energy propagates along the structure in both directions. Wave reflection occurs at the interface of two adjacent elements if they have different properties EI or ρA, which lead to different mechanical impedances. Wave reflection at these interfaces will interact with the incident wave to create resonance and antiresonance phenomena. To obtain the dereverberated response, wave reflection at any interface of adjacent elements must be suppressed. A series of controllers can be attached to both ends of each element to match the impedance of the two adjacent elements. Consider the left propagating wave first. When starting from node 3, energy passes element 3 to reach node 2. At node 2, the effect of controllers G_{3l} and G_{2l} permits the impedance of elements 2 and 3 to be matched. No energy reflection occurs at node 2. Thus, the entire energy will continue transmitting into element 2. When the wave reaches node 1, controllers G_{2l} and G_{1l} act together to make sure that no energy is reflected. At node 0, element 1 is free–free. The effect of controller G_{1l} is to extend element 1 to infinity. The energy continues transmitting to infinity. The result is that no energy reflection occurs across the part of structure to the left of input force F_3. A similar scenario occurs for wave transmitting to the right of input force F_3. Thus, the dereverberated response can be obtained for a nonuniform free–free beam structure using virtual control forces to prevent reflections. Both the conventional RTF and DTF responses are shown in Fig. 13. The properties of the beam used in this study are listed in Table 2.

$$\text{RTF}^{-1} = \begin{bmatrix} K_4^1 + K_1^2 & K_2^2 & & 0 & \\ K_3^2 & K_4^2 + K_1^3 & K_2^3 & & \\ & K_3^3 & K_4^3 + K_1^4 & K_2^4 & \\ & 0 & K_3^4 & K_4^4 + K_1^5 & K_2^5 \\ & & & K_3^5 & K_4^5 \end{bmatrix} \tag{40}$$

As shown earlier in the free–free case, the vertical displacement and angular displacement of each node are fed back into local controllers to generate control forces that can eliminate wave reflection at each node. In the case of fixed–free beam, controllers can be attached at all nodes except for the node at the fixed end. The DTF responses with respect to input F_3 can be obtained from the following expression:

$$\begin{bmatrix} v_1/F_3 \\ \theta_1/F_3 \\ v_2/F_3 \\ \theta_2/F_3 \\ v_3/F_3 \\ \theta_3/F_3 \\ v_4/F_3 \\ \theta_4/F_3 \\ v_5/F_3 \\ \theta_5/F_3 \end{bmatrix}_{\text{DTF}} = \left(\text{RTF}^{-1} + \begin{bmatrix} -K_4^1 + G_{2l} & & & & \\ & G_{3l} - G_{2l} & & 0 & \\ & & 0_{2\times 2} & & \\ & 0 & & G_{4r} - G_{5r} & \\ & & & & G_{5r} \end{bmatrix} \right)^{-1} \begin{bmatrix} 0 \\ 0 \\ 0 \\ 0 \\ 1 \\ 0 \\ 0 \\ 0 \\ 0 \\ 0 \end{bmatrix} \tag{41}$$

2. Fixed–Free Beam

Consider the fixed–free beam shown in Fig. 11b. The left end of the beam is fixed and the right end is free. Energy is input into this beam by means of $F_3 \neq 0$. The conventional RTF matrix of this five-element beam can be obtained experimentally. The inverse of the RTF is the dynamic stiffness matrix of the beam:

where K_4^1 can be obtained because the physical properties of the first element are known. The RTF and DTF responses are shown in Fig. 14.

When the expressions in Eqs. (39) and (41) are compared, the difference between the free–free beam and the fixed–free beam dereverberated responses depends on how the boundary conditions are

Table 2 Properties of the beam structure[a]

	Element				
Property	1	2	3	4	5
EI, N · m^2	4	1	10	2	3
ρA, kg/m	2	1	5	3	1
Length, m	2	3	3	1	1

[a]Assuming 0.01% damping.

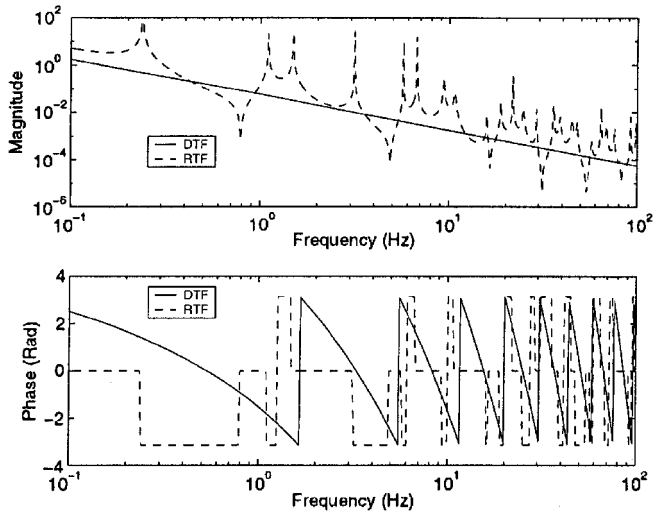

a) v_0/F_3

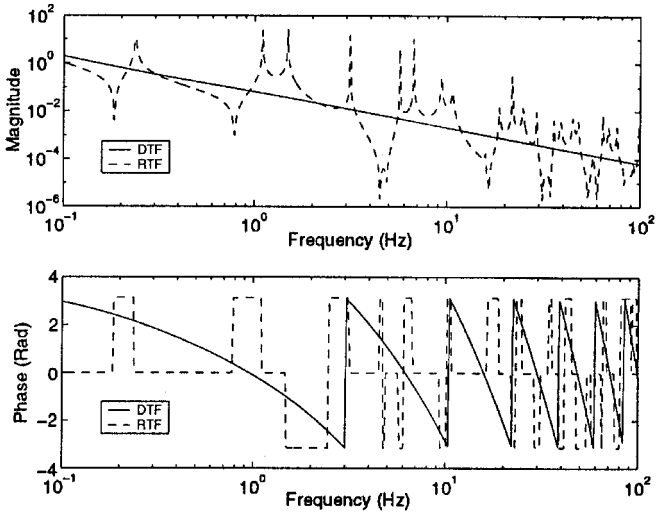

b) v_1/F_3

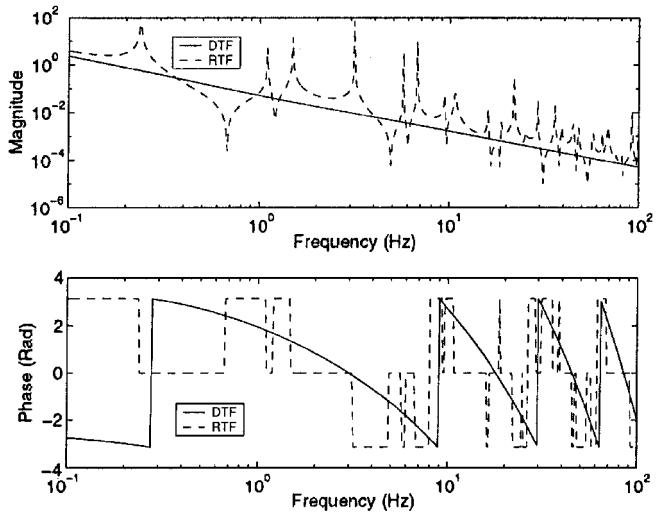

c) v_2/F_3

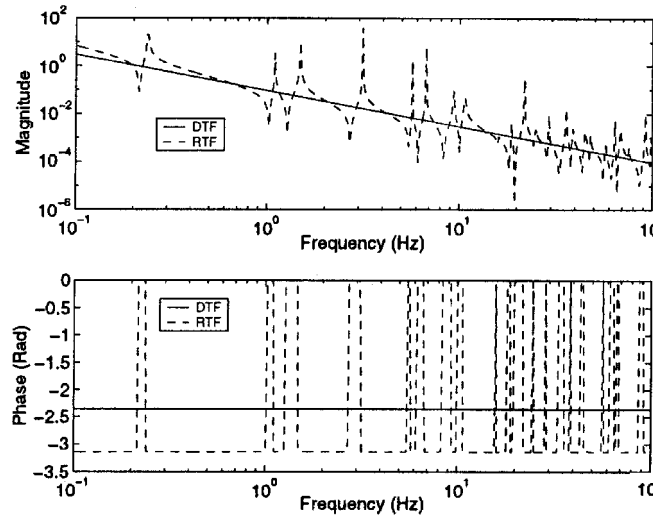

d) v_3/F_3

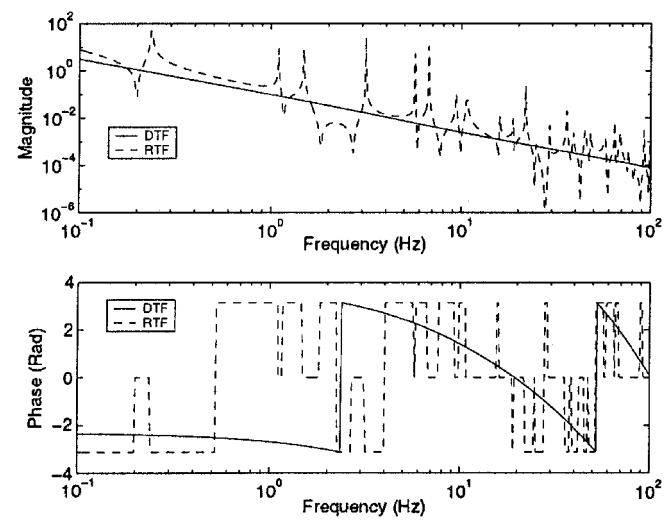

e) v_4/F_3

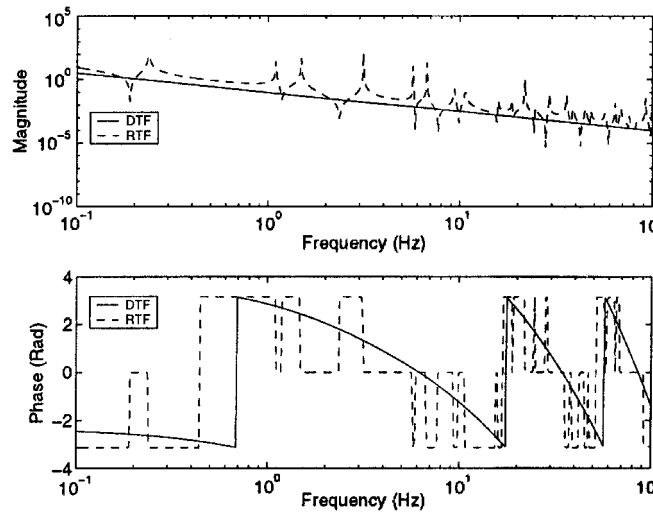

f) v_5/F_3

Fig. 13 DTF and RTF response of free–free beam structure.

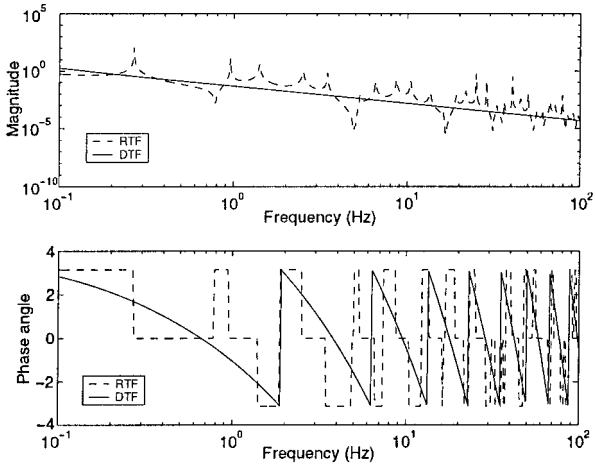

a) v_1/F_3

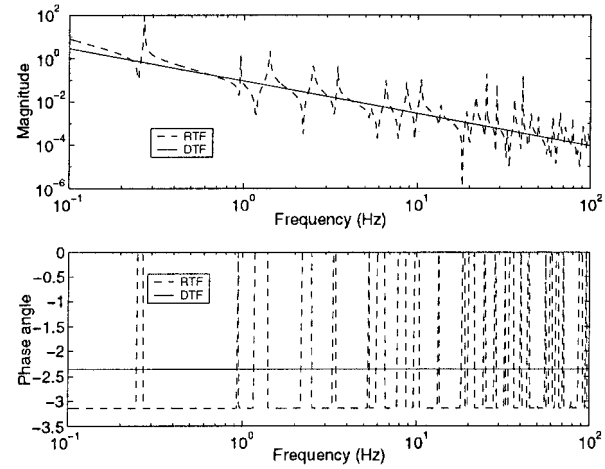

c) v_3/F_3

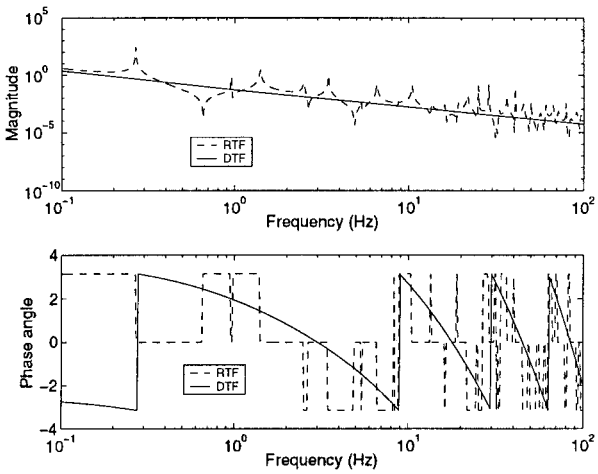

b) v_2/F_3

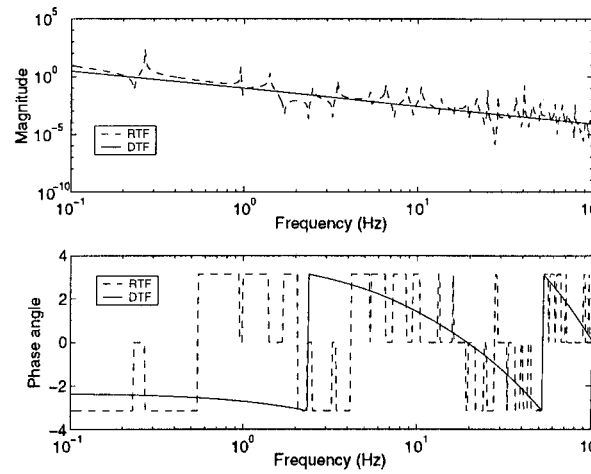

d) v_4/F_3

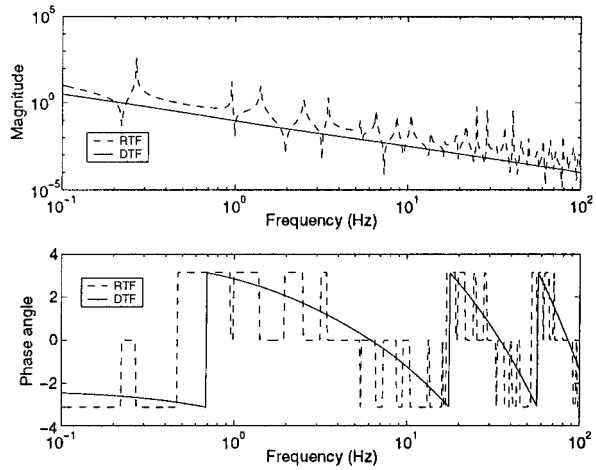

e) v_5/F_3

Fig. 14 DTF and RTF response of fixed–free beam structure.

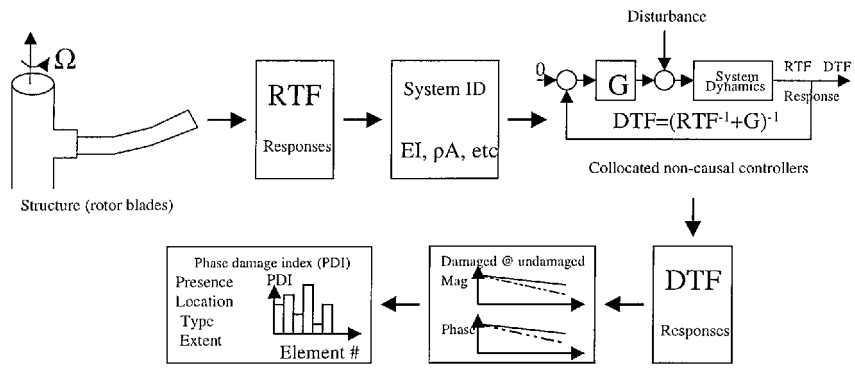

Fig. 15 Damage detection methodology based on DTF response.

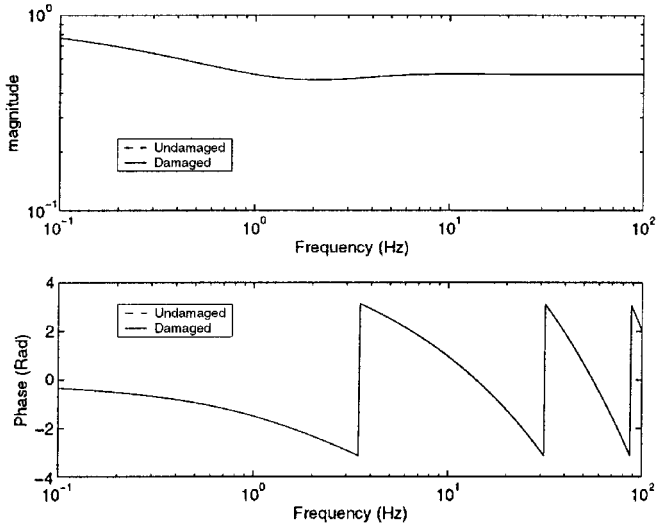

a) DTF response v_1/v_0

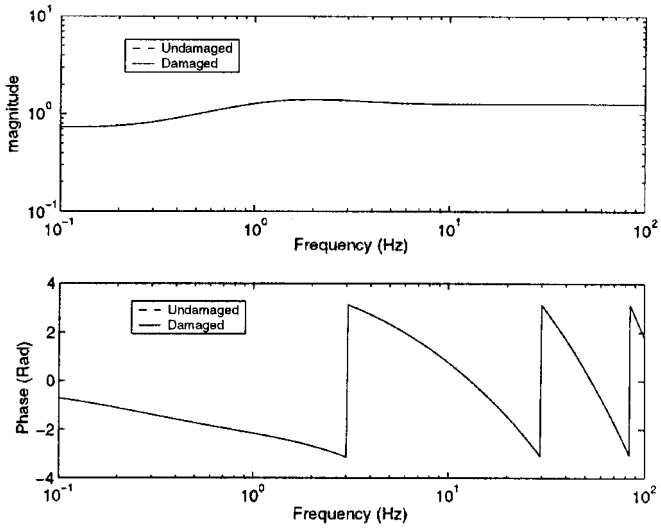

b) DTF response v_2/v_1

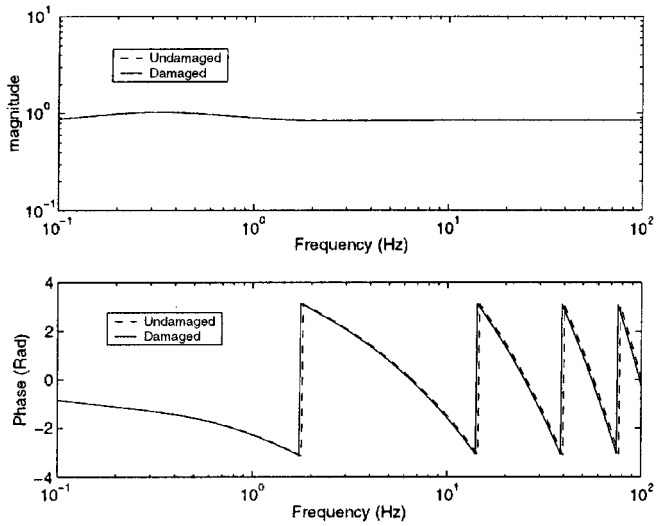

c) DTF response v_3/v_2

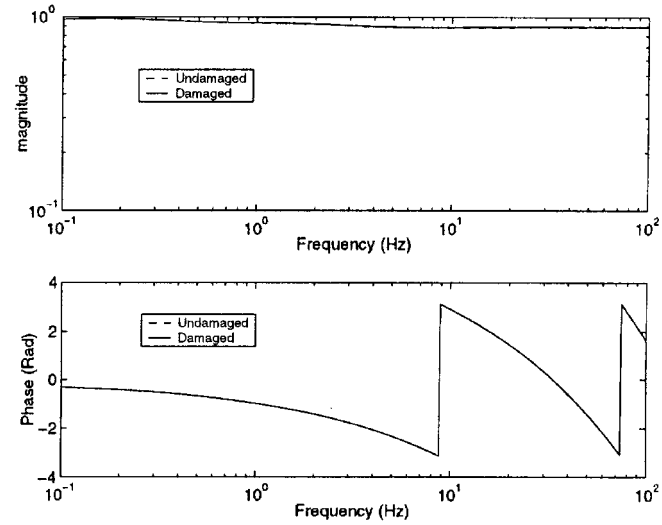

d) DTF response v_4/v_3

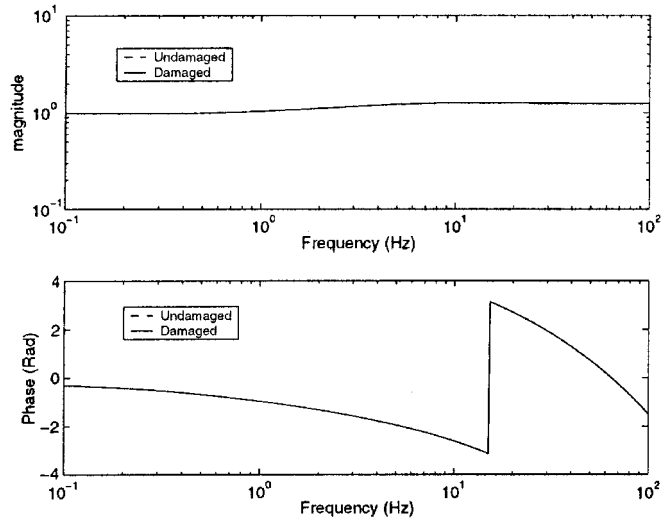

e) DTF response v_5/v_4

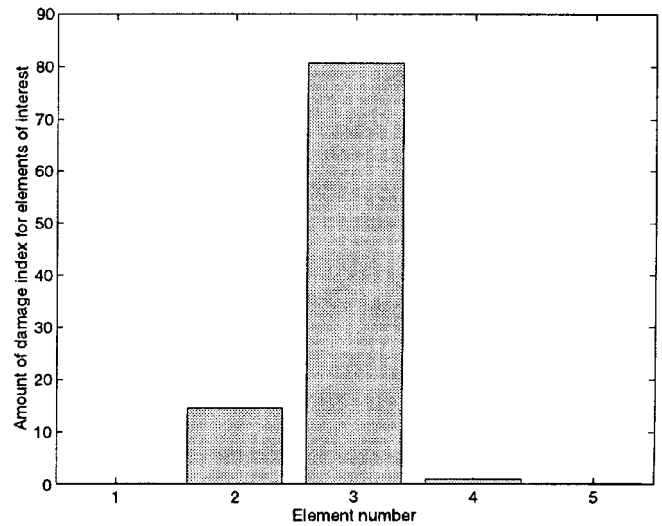

f) Damage index (PDI) vs element number

Fig. 16 Element 3 damage in terms of 5% loss in stiffness.

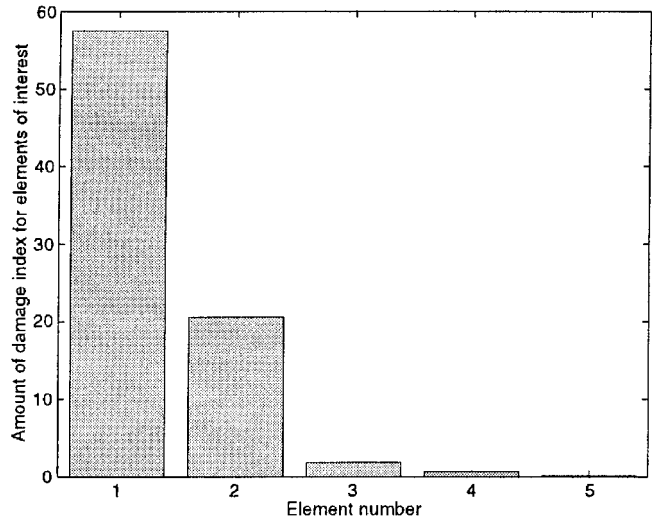

a) Element 1 damaged (5% stiffness loss)

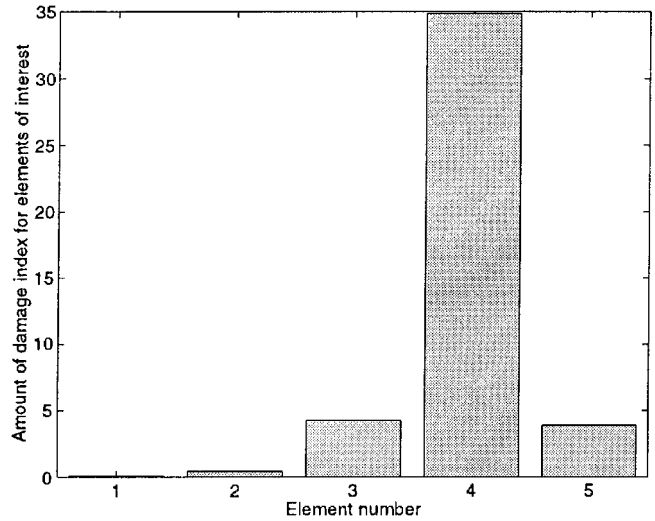

c) Element 4 damaged (5% stiffness loss)

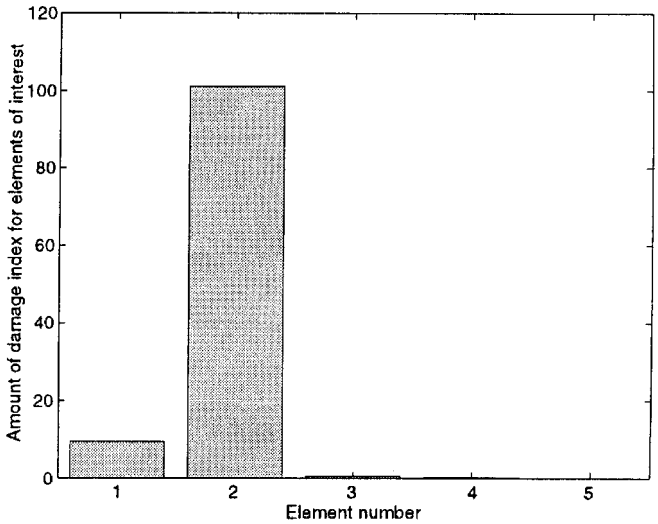

b) Element 2 damaged (5% stiffness loss)

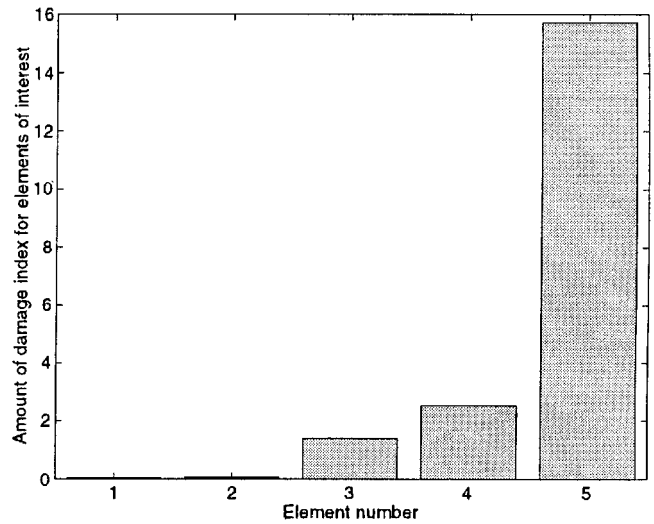

d) Element 5 damaged (5% stiffness loss)

Fig. 17 Damage index (PDI) vs element number.

treated. For the free–free beam, a controller is needed to extend the free end to infinity. However, for the fixed–free beam, element 1 is ignored, and element 2 needs to be extended to the left to infinity. To achieve this, K_4^1 is the affecting part from element 1 and G_{2l} is from element 2.

IV. Damage Detection Approach Based on DTF Response

A. Detecting Presence and Location of Damage

In the preceding section, collocated noncausal controllers were developed to obtain the DTF responses for discrete spring–mass structural elements and spectral rod and beam finite elements. In this section, a methodology for detecting damage in one-dimensional structures is developed based on the characteristic changes in the DTF responses. For an undamaged structure, collocated noncausal controllers can be developed based on an identified model of the structural system. Implementing these noncausal controllers offline in a computer will yield the DTF response from each actuator to each sensor. To infer the presence of damage, these undamaged controllers can be repeatedly applied to the identified RTF responses of a structural system. Thus, as damage appears in the structure, its presence will be revealed in the magnitude and phase plots of the DTF responses. Therefore, by the tracking of relative magnitude and phase errors between the undamaged and damaged structure's DTF response, it is possible to infer both the presence and location of damage. Furthermore, to determine damage in a particular structural element, one only needs to track the transmission of incident energy through the structure. This can be done by computing the ratio of the DTF responses for sequential DOF. This damage detection methodology is shown in Fig. 15.

By the use of examples of a free–free and fixed–free beam, the concept of a phase damage index is introduced to illustrate how the presence, location, type, and amount of damage can be determined.

1. *Free–Free Beam*

Consider the free–free beam structure shown in Fig. 11a. Energy is input at node 3 with external force $F_3 \neq 0$. Figure 16 shows the DTF responses for the following transmission ratio of sequential degrees of freedom: v_1/v_0, v_2/v_1, v_3/v_2, ... The solid line refers to the undamaged case, and the dashed line refers to the damaged case. Each part of Fig. 16 shows the respective magnitude and phase response of the transmission ratio. It has been assumed that damage in the form of a loss of stiffness is simulated in element 3. Careful inspection of Fig. 16 suggests two observations: First, in the case of stiffness damage, the phase of the DTF response will wrap around $-\pi$ earlier than in the undamaged case. Second, there is not a significant change in the DTF magnitude response due to the presence of damage in the structure. To explain these observations in more detail, one has to consider the effect of damage on the structure's wave propagation response. When a leftward propagating wave passes through a damaged element such as element 3, the effect of a stiffness loss is to increase the wave number and slow down the propagation of

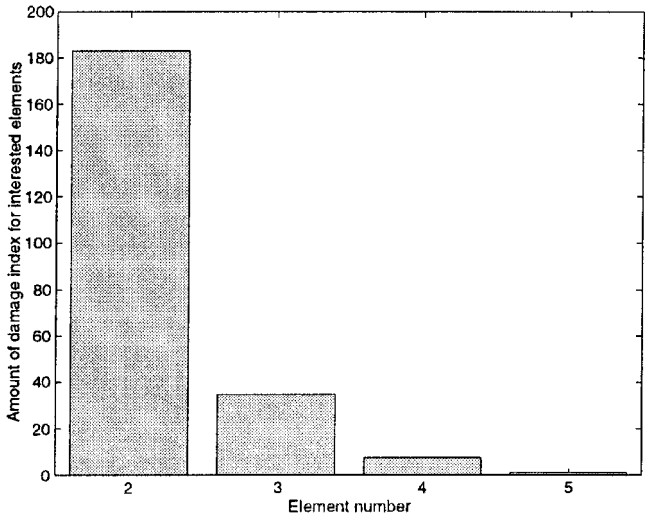

a) Element 1 damaged (5% stiffness loss)

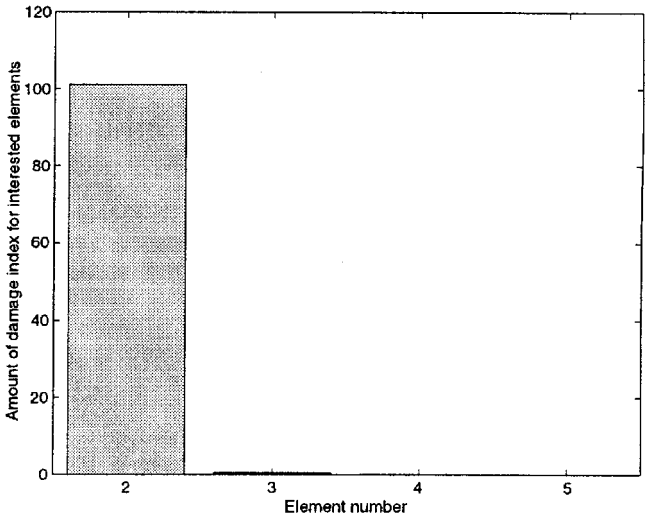

b) Element 2 damaged (5% stiffness loss)

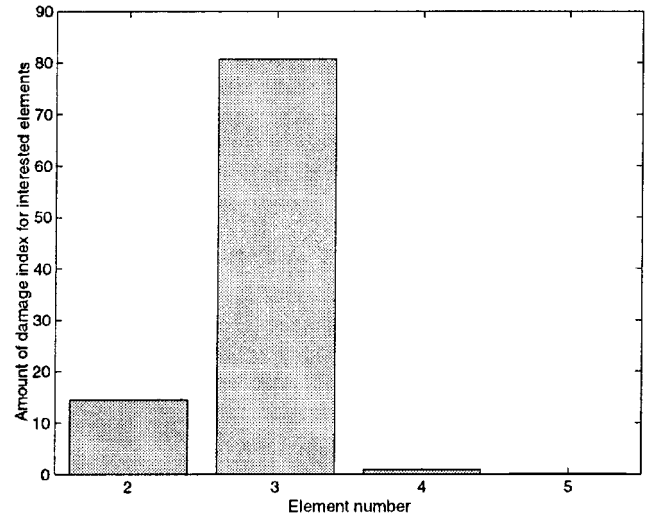

c) Element 3 damaged (5% stiffness loss)

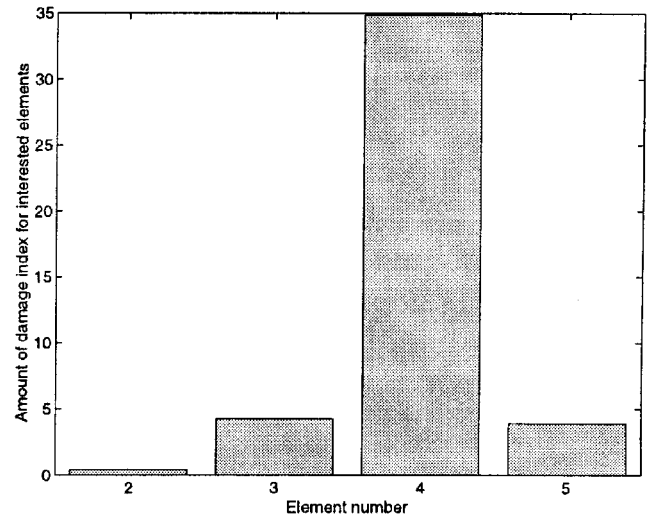

d) Element 4 damaged (5% stiffness loss)

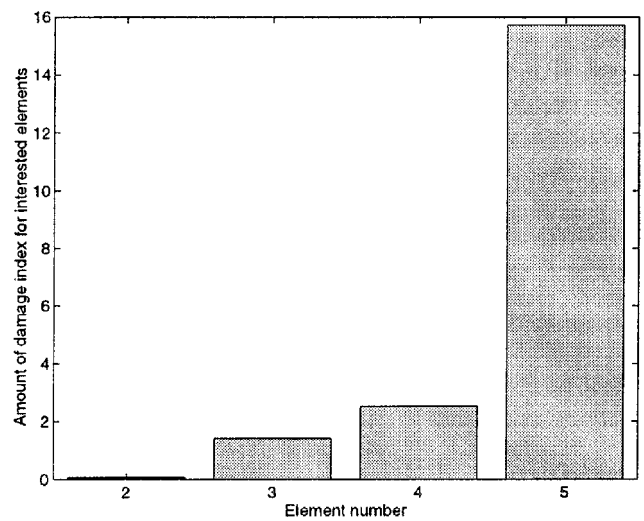

e) Element 5 damaged (5% stiffness loss)

Fig. 18 Damage indices (PDI) vs element number.

the transmitted wave. This introduces an additional phase lag in the DTF response. Undamaged structural elements have no effect on the propagation of the transmitted wave. In terms of the magnitude response, the noncausal controllers are designed to prevent wave reflection at the interfaces between structural elements. However, when damage occurs, wave reflection is not prevented because the controllers can no longer provide a matched terminating boundary condition at each end. Nevertheless, because the simulated damage is small, the magnitude of the DTF displays a modest sensitivity to damage. Therefore, a phase damage index (PDI) has been developed to locate the element that contains the damage. The PDI is based on the relative phase error from successive DOF and is given by

$$\mathrm{PDI}_n = \sum_{\omega_l \le \omega \le \omega_u} \left| \mathrm{phase}\left(\frac{v^n}{v^{n-1}}(\omega)\right)_{\mathrm{DTF}}^{\mathrm{undamaged}} - \mathrm{phase}\left(\frac{v^n}{v^{n-1}}(\omega)\right)_{\mathrm{DTF}}^{\mathrm{damaged}} \right| \tag{42}$$

where $n = 1, 2, \ldots, 5$ refers to the ith element and ω_l and ω_u are the lower and upper bounds of the frequency range of interest. Computing the value of the PDI for each structural element indicates which element is damaged. This is evident from the PDI computed for the free–free beam example described earlier in this section. Notice that the PDI is significantly larger for element 3 in which simulated stiffness damage was assumed (Fig. 16f). Figure 17 shows the PDI for assumed stiffness damage in each of the other four structural elements. Notice that in all cases the PDI with the largest absolute value indicates the structural element that is damaged in the free–free beam example.

2. Fixed–Free Beam

For a fixed–free beam,

$$\begin{pmatrix} v_0 \\ \theta_0 \end{pmatrix} = \begin{pmatrix} 0 \\ 0 \end{pmatrix}$$

Only $n = 2$, 3, 4, and 5 can be substituted into Eq. (42) and four damage indices, PDI_2, PDI_3, PDI_4, and PDI_5, can be formulated. They are associated with elements 2, 3, 4, and 5, respectively. Five damage cases are simulated. Figure 18a shows damage indices vs element number when element 1 is damaged. Remember no damage index is formulated for element 1. However, from Fig. 18a, the index associated with element 2, PDI_2, is large. This implies that damage occurred in element 1, demonstrated by the damage index associated with element 2. Of course, from Fig. 18b, damage in element 2 leads to blowup of PDI_2, too. Therefore, if damage index of element 2 PDI_2 exhibits some large value, both elements 1 and 2 need to be checked to see whether they are damaged. The damage index of element 3, 4, and 5 can locate the damage of its associated element as shown in Figs. 18c, 18d, and 18e.

B. Damage Type and Extent

Most structural damage can be categorized as mass or stiffness related. In the case of the stiffness loss, the phase curve of the DTF response of a damaged structure tends to wrap at π or $-\pi$ earlier than in the undamaged case. In the case of the mass loss, the phase of the DTF response of a damaged structure tends to wrap later than in the undamaged case (Fig. 19). This pattern in the phase behavior for stiffness or mass damage is primarily a result of how wave number variations affect the transmission properties of an incident wave through a structural element. Thus, by the simply examination of the phase behavior of undamaged and damaged DTF responses, it is possible to ascertain the type of damage, albeit stiffness or mass. In addition, damping effects can also be identified.

Whereas the type of damage in a structural system can be determined from the phase response of the DTF, determining the extent of damage in a structural element is a bit more dificult. The PDI described earlier represents a qualitative measure of damage in a structure. However, by the conducting of a numerical study on the identified structural model, one can simulate structural damage in each structural element and correlate the PDI with percentage damage. Thus, a lookup table or curve-fitted database can be developed for each structural element to provide an estimate of the amount of damage in that element. Figure 20 shows such a correlation for the fixed–free beam example developed in Sec. IV.A.2. Notice that the PDI increases with structural damage in the structural element of interest. Similar trends exist for other elements.

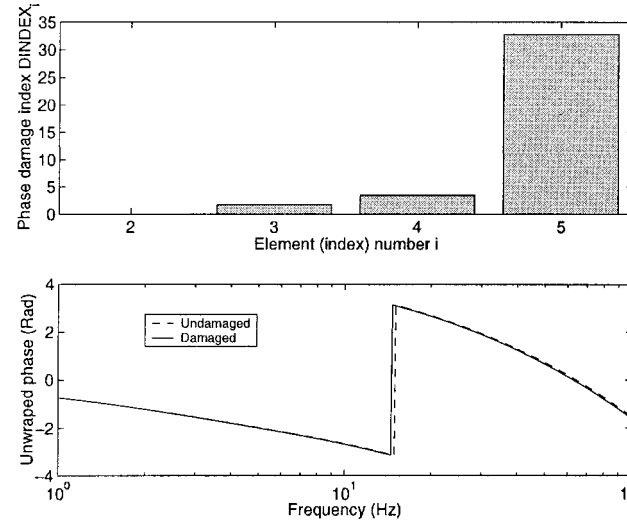

a) Element 5 damaged in terms of 5% loss in stiffness

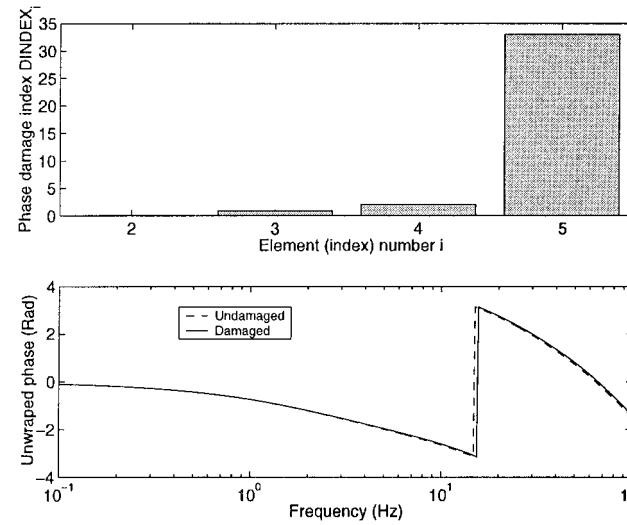

b) Element 5 damaged in terms of 5% loss in mass

Fig. 19 Fixed–free beam; energy input at node 3.

V. Discussion

1) The damage detection methodology presented requires a fully populated transfer function matrix. For the real-life structure, these transfer functions can be obtained by attaching sensors along the structure at each DOF and moving the excitation actuator along the structure. The ratio between sensor output and actuator input is conventional RTF. Although moving the excitation force location is unrealistic, system identification can be used to obtain a fully populated RTF matrix.

2) Because DTF is based on measured RTF, the test effort is comparable to that of conventional RTF, which is well known to researchers in this field. As for the exact computational effort, it depends on the number of DOF defined in the problem, plus the number of frequency points included in the calculation. Table 3 shows computational efforts involved in the examples of this paper.

3) The test instrumentation and type of measurements needed for DTF is identical to those required for conventional RTF. These include conventional sensors such as accelerometers, strain gauges, linear variable displacement transducers (LVDTs), and actuators such as shakers and hydraulic test systems.

Table 3 Computational effort to obtain DTF

Example (500 frequency points)	CPU time, s
5-DOF spring–mass system	7.8410
Fixed–free beam	17.8560
Free–free beam	16.8340

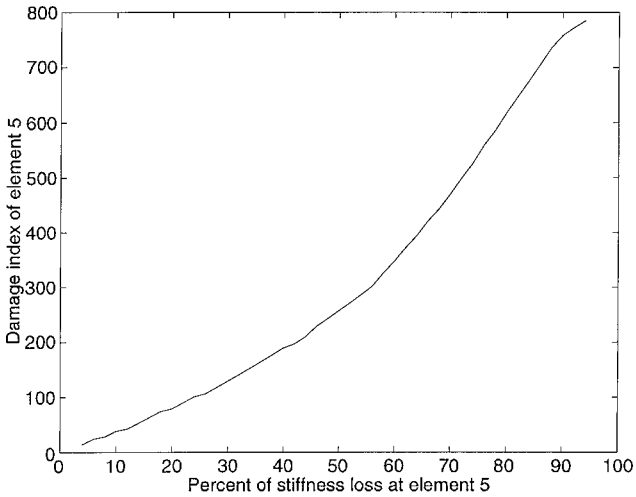

Fig. 20 Fixed–free beam, fifth element damaged; PDI_5 vs percent of stiffness loss at element 5.

VI. Summary

This paper has introduced a wave propagation approach for computing the DTF responses on nonuniform structures. With the use of the DTF responses, boundary effects are ignored in favor of the incident path that the energy takes to travel through a structure. The DTF responses, associated with an individual element, has been shown to be sensitive to physical parameter changes that are directly in the load path from input force to measured sensor response. The DTF appears to provide direct information regarding the source, location, and amount of damage.

Acknowledgments

This work was supported by the National Science Foundation under Grant CMS9625004, with S. C. Liu and William Anderson serving as Contract Monitors.

References

[1]Doebling, S. W., Farrar, C. R., Prime, M. B., and Shevitz, D. W., "Damage Identification and Health Monitoring of Structural and Mechanical Systems from Changes in Their Characteristics: A Literature Review," Los Alamos National Lab., Rept. LA-13070-MS, Los Alamos, NM, June 1995.

[2]Farrar, C. R., and Jauregui, D. A., "Comparative Study of Damage Identification Algorithms Applied to a Bridge: I Experiment," *Smart Materials and Structures*, Vol. 7, No. 5, 1998, pp. 704–719.

[3]Farrar, C. R., and Jauregui, D. A., "Comparative Study of Damage Identification Algorithms Applied to a Bridge: II Numerical Study," *Smart Materials and Structures*, Vol. 7, No. 5, 1998, pp. 720–731.

[4]Chang, F. K., *The Proceedings of the Second International Workshop on Structural Health Monitoring*, Stanford Univ., Stanford, CA, 1999.

[5]Doyle, J. F., "Determining the Size and Location of Transverse Cracks in Beams," *Experimental Mechanics*, Vol. 35, 1995, pp. 272–280.

[6]Lakshmanan, K. A., and Pines, D. J., "Damage Identification of Chordwise Crack Size and Location in Uncoupled Composite Rotorcraft Flexbeams," *Journal of Intelligent Materials and Systems and Structures*, Vol. 9, No. 1, 1998, pp. 146–155.

[7]von Flotow, A. H., and Schafer, B., "Wave-Absorbing Controllers for a Flexible Beam," *Journal of Guidance, Control, and Dynamics*, Vol. 19, 1986, pp. 673–680.

[8]Pines, D. J., and von Flotow, A. H., "Active Control of Bending Wave Propagation at Acoustic Frequencies," *Journal of Sound and Vibration*, Vol. 142, No. 3, 1990, pp. 391–412.

[9]MacMartin, D. G., and Hall, S. R., "Control of Uncertain Structure Using an h_∞ Power Flow Approach," *Journal of Guidance, Control, and Dynamics*, Vol. 14, No. 3, 1991, pp. 521–530.

[10]Miller, D. W., and Hall, S. R., "Experimental Results Using Active Control of Traveling Wave Power Flow," *Journal of Guidance, Control, and Dynamics*, Vol. 14, No. 2, 1991, pp. 91–98.

[11]Matsuda, K., and Fujii, H. A., "Analysis of Dereverberated Transfer Function in Finite Dimensions," *Journal of Guidance, Control, and Dynamics*, Vol. 19, No. 1, 1996, pp. 91–98.

[12]Betros, R. S., Alvarez-Salazar, O. S., and Bronowicki, A. J., "Experiences with Active Damping and Impedance Matching Compensators," *Proceedings of the 1993 Smart Structures and Intelligent Systems Conference*, Vol. 1917, Society of Photo-Optical Instrumentation Engineers, Bellingham, WA, 1993, pp. 856–869.

[13]Purekar, A., and Pines, D. J., "Detecting Damage in Non-uniform Beams Using the Dereverberated Transfer Function Response," *Smart Materials and Structures*, Vol. 9, No. 4, 2000, pp. 429–444.

[14]Brillouin, L., *Wave Propagation in Periodic Structures*, 2nd ed., Dover, New York, 1946.

[15]Doyle, J. F., *Wave Propagation in Structures*, 2nd ed., Springer, New York, 1997.

A. Berman
Associate Editor